

# One Step Is Enough: Dispersive MeanFlow Policy Optimization

Guowei Zou<sup>1,2</sup> Haitao Wang<sup>1,2</sup> Hejun Wu<sup>1,2</sup> Yukun Qian<sup>1,2</sup> Yuhang Wang<sup>1,2</sup> Weibing Li<sup>1,2</sup>

## Abstract

Real-time robotic control demands fast action generation. However, existing generative policies based on diffusion and flow matching require multi-step sampling, fundamentally limiting deployment in time-critical scenarios. We propose Dispersive MeanFlow Policy Optimization (**DMPO**), a unified framework that enables true one-step generation through three key components: MeanFlow for mathematically-derived single-step inference without knowledge distillation, dispersive regularization to prevent representation collapse, and reinforcement learning (RL) fine-tuning to surpass expert demonstrations. Experiments across RoboMimic manipulation and OpenAI Gym locomotion benchmarks demonstrate competitive or superior performance compared to multi-step baselines. With our lightweight model architecture and the three key algorithmic components working in synergy, DMPO exceeds real-time control requirements ( $>120\text{Hz}$ ) with **5–20× inference speedup**, reaching hundreds of Hertz on high-performance GPUs. Physical deployment on a Franka-Emika-Panda robot validates real-world applicability. **Code is available at <https://guowei-zou.github.io/dmopo-page/>.**

## 1. Introduction

Real-time control is essential for dexterous robotic manipulation, requiring fast action generation to ensure smooth and responsive behavior. Generative models based on diffusion and flow matching have achieved remarkable success in modeling complex, multimodal action distributions (Chi et al., 2023; Ze et al., 2024; Zhang et al., 2025a), yet their multi-step sampling procedures incur significant latency per action, fundamentally limiting deployment in time-critical

<sup>1</sup>School of Computer Science and Engineering, Sun Yat-sen University, Guangzhou, China <sup>2</sup>Guangdong Key Laboratory of Big Data Analysis and Processing, Guangzhou, China. Email: {zougw, qianyk5, wangyh253}@mail2.sysu.edu.cn; {wanght39, wuhejun, liwb53}@mail.sysu.edu.cn.

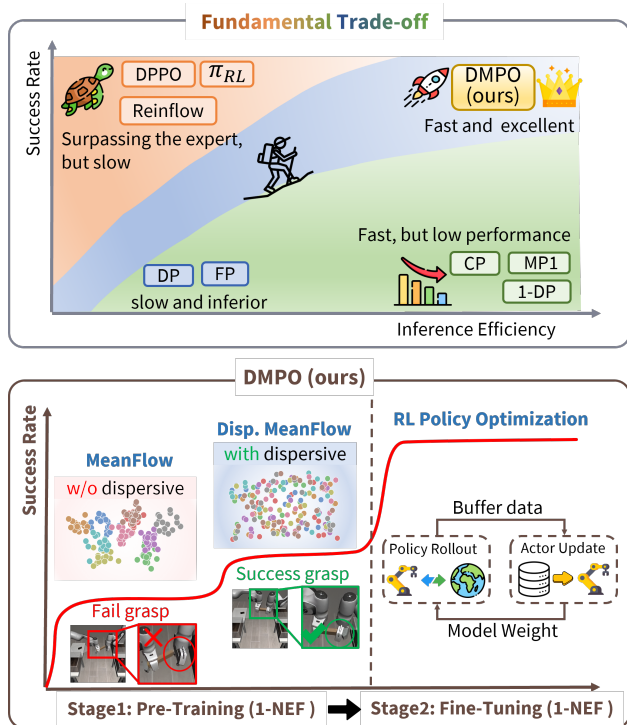


Figure 1. From efficiency–performance trade-off to practical real-time control. **Top:** Existing methods lie on the trade-off curve: multi-step approaches (DPPO, ReinFlow,  $\pi_{RL}$ ) achieve strong performance but slow inference, while one-step methods (CP, MP1, 1-DP) are fast but unstable. DMPO breaks this trade-off by occupying the upper-right region. **Bottom:** DMPO’s two-stage approach: dispersive MeanFlow prevents representation collapse during pre-training, and PPO fine-tuning enables adaptation beyond demonstrations.

scenarios. This motivates the pursuit of one-step generation policies that can match multi-step quality while enabling real-time control. However, existing methods face three interconnected challenges: (1) *inference efficiency*, where multi-step sampling in diffusion and flow-based policies incurs significant latency, while distillation-based one-step methods like CP (Prasad et al., 2024) and 1-DP (Wang et al., 2025) require complex training pipelines (Lu et al., 2024; Yan et al., 2025; Clemente et al., 2025); (2) *representation collapse*, where one-step generation methods risk mapping distinct observations to indistinguishable representations, degrading action quality with no opportunity for iterative

correction (Wang & He, 2025; Zou et al., 2026); (3) *performance ceiling*, since pure imitation learning cannot surpass expert demonstrations, yet reinforcement learning (RL) fine-tuning (Ren et al., 2025; Zhang et al., 2025b; Chen et al., 2025b) is impractical with slow multi-step inference and unstable with collapsed representations. These challenges form a coupled loop: fast inference requires one-step generation, stable one-step generation requires preventing collapse, breaking the performance ceiling requires RL fine-tuning, and efficient RL fine-tuning requires both fast inference and high-quality representations. Any method addressing only one challenge will be blocked by the others, as illustrated in Fig. 1.

We propose Dispersive MeanFlow Policy Optimization (**DMPO**), which resolves this coupled problem through three mutually supporting components. MeanFlow one-step generation (Geng et al., 2025a) provides mathematically rigorous single-step inference without distillation, establishing the foundation for real-time control and efficient fine-tuning. Dispersive regularization (Wang & He, 2025) prevents representation collapse, ensuring one-step generation stability while providing high-quality initialization for subsequent RL fine-tuning. RL fine-tuning (Zhang et al., 2025b) breaks through imitation learning’s performance ceiling, enabling policies to surpass expert data, while one-step inference efficiency makes large-scale fine-tuning practical. These components form a positive feedback loop: dispersive regularization makes one-step generation stable, one-step generation makes RL fine-tuning efficient, and high-quality pre-training provides a good starting point for RL, ultimately achieving a one-step policy that is both fast and effective.

Our contributions are: (1) **Framework**: We introduce DMPO, the first framework that breaks the efficiency-performance trade-off in generative robot policies, achieving  $5\text{--}20\times$  speedup while matching or exceeding multi-step baselines. (2) **Theory**: We establish the first information-theoretic foundation proving dispersive regularization is necessary for stable one-step generation (Appendix D), and derive the first mathematical formulation for RL fine-tuning of one-step policies (Appendix C). (3) **Validation**: We achieve state-of-the-art on RoboMimic (Mandlekar et al., 2021) and OpenAI Gym (Brockman et al., 2016), and validate real-time control ( $>120\text{Hz}$ ) on a Franka-Emika-Panda robot.

## 2. Related Work

We organize related work according to the three categories identified in the introduction.

### 2.1. Multi-Step Generative Policies

Diffusion Policy (Chi et al., 2023) pioneered visuomotor control via denoising diffusion, with DP3 (Ze et al., 2024)

extending to 3D inputs. Flow matching (Lipman et al., 2023; Boffi et al., 2025) and Rectified Flow (Liu et al., 2023) offer alternatives through learned velocity fields, applied in Flow Policy (Zhang et al., 2025a), shortcut flows (Chen et al., 2025c), and foundation models  $\pi_0$  (Team, 2024),  $\pi_{0.5}$  (Team, 2025). Despite expressiveness, these methods require tens to hundreds of NFEs per action and cannot exceed expert performance through imitation learning alone.

### 2.2. One-Step Generation Methods

Consistency Policy (Prasad et al., 2024) and 1-DP (Wang et al., 2025) reduce generation to one step via distillation but remain bounded by teacher capability (Lu et al., 2024; Yan et al., 2025; Clemente et al., 2025; Chen et al., 2025a; Liu et al., 2025a). MP1 (Sheng et al., 2026) is the first to apply MeanFlow (Geng et al., 2025a;b; Guo et al., 2025; Hu et al., 2025) for distillation-free one-step generation, demonstrating that averaged-velocity flow models can be deployed without a diffusion teacher. However, one-step generation tends to collapse intermediate representations. Although dispersive regularization has been applied to multi-step diffusion models (Wang & He, 2025; Zou et al., 2026) to improve representation quality, its application to distillation-free one-step policies remains unexplored. We present the first study applying dispersive regularization to MeanFlow for stable one-step generation.

### 2.3. RL Fine-tuning for Generative Policies

DPPO (Ren et al., 2025) pioneered RL fine-tuning for diffusion policies (Schulman et al., 2017), ReinFlow (Zhang et al., 2025b) extended this to flow-based policies, and  $\pi_{RL}$  (Chen et al., 2025b) further scaled RL for VLAs (Lu et al., 2025; Liu et al., 2025b; McAllister et al., 2025). However, all operate on multi-step policies, inheriting computational overhead (Zou et al., 2026; Wagenmaker et al., 2025). Moreover, RL fine-tuning can be unstable, where performance degrades as training progresses. Behavior cloning regularization (Nair et al., 2021) mitigates this by preventing catastrophic forgetting. DMPO fills the gap by developing stable RL fine-tuning for true one-step policies.

## 3. Methodology

This section presents the DMPO methodology. We first provide a framework overview in Section 3.1, then detail our three contributions: MeanFlow one-step generation in Section 3.2, dispersive regularization in Section 3.3, and RL fine-tuning with BC regularization in Section 3.4. Detailed mathematical derivations are provided in Appendix C. Figure 2 presents the complete DMPO pipeline, organized as two stages. **Our core design philosophy is to achieve true real-time robotic control by combining a lightweight model architecture with complementary algorithm design.**

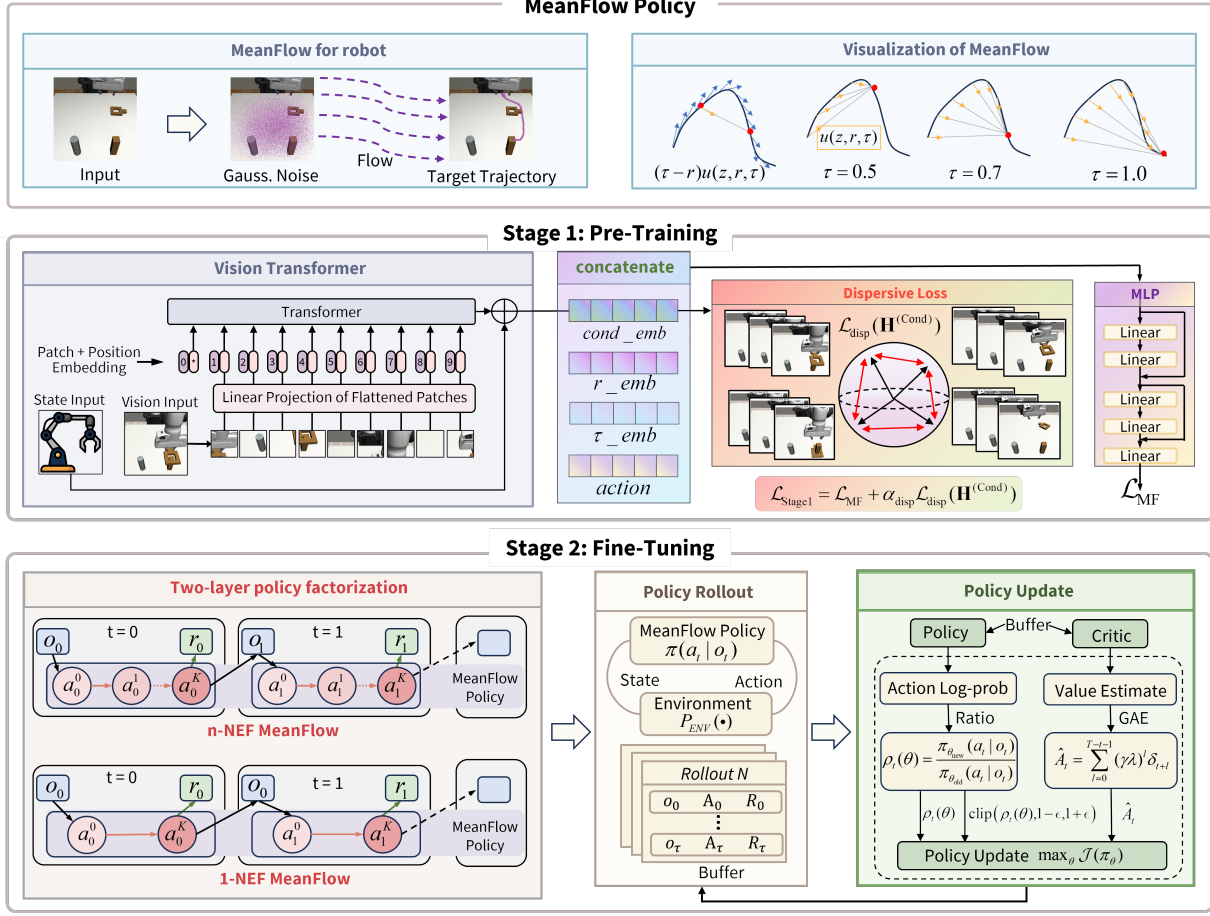


Figure 2. DMPO Framework Overview. **Stage 1 (Top & Middle):** Pre-training with dispersive MeanFlow. MeanFlow learns velocity fields that transform noise into actions via Vision Transformer encoding with dispersive losses to prevent representation collapse. **Stage 2 (Bottom):** PPO fine-tuning formulated as a two-layer policy factorization: the outer layer is the true environment MDP, while the inner latent chain only reparameterizes the action distribution.

### 3.1. Framework Overview

**Lightweight Architecture for Real-Time Control.** Following prior robotic learning work (Peroldi et al., 2021), we adopt a single-layer light ViT with 128-dimensional embeddings combined with an MLP action head, totaling only 1.78M parameters (48× smaller than ViT-Base). This compact design enables inference speeds exceeding 120Hz for real-time control.

**Stage 1: Pre-Training DMPO.** The top and middle panels illustrate pre-training. MeanFlow learns a velocity field  $u(z, s, \tau)$  that transforms Gaussian noise into action trajectories, enabling few-step or one-step sampling. Visual inputs are processed by a Vision Transformer and fused with robot state into the conditional embedding. An MLP processes this embedding along with time embeddings to predict velocity fields. Dispersive loss is applied to the conditional embedding to prevent representation collapse.

**Stage 2: RL Fine-Tuning DMPO.** The bottom panel shows

the fine-tuning stage. We adopt a *two-layer policy factorization*: the outer layer is the actual environment MDP with rewards and visitation frequencies, whereas the inner layer contains the latent denoising chain  $a^{K-1} \rightarrow \dots \rightarrow a^0$  that merely reparameterizes  $\pi_\theta(a | o)$ . Since latent states neither interact with the environment nor generate rewards, PPO advantages and value targets are always defined on the outer environment. Policy updates follow PPO with clipped probability ratios  $\rho_t(\theta)$  and GAE advantages  $\hat{A}_t$ , while behavior cloning regularization prevents catastrophic forgetting.

### 3.2. One-Step Generation Policy in DMPO

MeanFlow extends flow matching by learning an *average velocity field* rather than instantaneous velocities. Given linear interpolation  $z_\tau = (1 - \tau)a + \tau\epsilon$  between target action  $a$  (at  $\tau=0$ ) and noise  $\epsilon \sim \mathcal{N}(0, I)$  (at  $\tau=1$ ), the average velocity over interval  $[r, \tau]$  is:

$$u(z_\tau, r, \tau) \triangleq \frac{1}{\tau - r} \int_r^\tau v(z_\xi, \xi) d\xi, \quad (1)$$

satisfying the displacement identity  $(\tau - r)u(z_\tau, r, \tau) = z_\tau - z_r$ . Differentiating yields the **MeanFlow identity**:

$$u(z_\tau, r, \tau) = v(z_\tau, \tau) - (\tau - r) \frac{d}{d\tau} u(z_\tau, r, \tau), \quad (2)$$

where the total derivative  $\frac{d}{d\tau} u = v_\tau \cdot \nabla_z u + \partial_\tau u$  involves a Jacobian-vector product (JVP, see Eq. 20 in Appendix C.1). The MeanFlow training objective is:

$$\mathcal{L}_{\text{MF}} = \mathbb{E}_{(o, a), \epsilon, (r, \tau)} \left[ \|u_\theta(z_\tau, r, \tau, o) - u_{\text{tgt}}\|^2 \right], \quad (3)$$

where  $u_{\text{tgt}} = v_\tau - (\tau - r) \frac{d}{d\tau} u_\theta$  is the target velocity (Eq. 21), and  $v_\tau = \epsilon - a$  is the instantaneous velocity pointing from data to noise. Complete formulations including JVP computation and time sampling strategies are provided in Appendix C.1.

### 3.3. Dispersive Regularization for Preventing Collapse in One-Step Generation Policy

MeanFlow suffers from *representation collapse* where distinct observations map to similar embeddings. We identify two contributing factors: (1) the averaged velocity training objective is less sensitive to fine-grained representation differences, and (2) few-step inference amplifies this issue by providing limited opportunities to query the representation. Detailed theoretical analysis is provided in Appendix D.1. Dispersive regularization addresses the root cause by encouraging intermediate features  $\mathbf{H} = \{\mathbf{h}_1, \dots, \mathbf{h}_K\} \subset \mathbb{R}^d$  to spread in feature space. We explore four formulations: (1) **InfoNCE-L2** maximizes pairwise L2 distances via contrastive learning:

$$\mathcal{L}_{\text{InfoNCE-L2}} = -\mathbb{E} \left[ \log \frac{\exp(\|\mathbf{h}_i\|_2^2 / \tau)}{\sum_{k \neq i} \exp(-\|\mathbf{h}_i - \mathbf{h}_k\|_2^2 / \tau)} \right] \quad (4)$$

where  $\tau > 0$  is the temperature parameter. We also explore (2) **InfoNCE-Cosine** for angular separation, (3) **Hinge Loss** for minimum separation margin, and (4) **Covariance-Based** loss for feature decorrelation. Detailed formulations are provided in Appendix C.2.

The Stage 1 training objective combines MeanFlow and dispersive regularization:

$$\mathcal{L}_{\text{Stage1}} = \mathcal{L}_{\text{MF}} + \alpha_{\text{disp}} \mathcal{L}_{\text{disp}}(\mathbf{H}^{(\text{Cond})}), \quad (5)$$

where  $\alpha_{\text{disp}} > 0$  is the balancing coefficient, and we apply dispersive regularization to the **conditional embedding**  $\mathbf{H}^{(\text{Cond})}$  output by the Vision Transformer encoder. The conditional embedding encodes observation information (visual features and robot state) and is the key representation

for distinguishing different samples. Our analysis shows that dispersive regularization on the conditional embedding effectively mitigates representation collapse in few-step inference. Detailed discussion is provided in Appendix D.1.

### 3.4. RL Fine-tuning for One-Step Generation Policies

Pure imitation learning cannot surpass expert demonstrations. We address this through PPO fine-tuning with behavior cloning (BC) regularization.

**Stochastic Sampling.** During fine-tuning, we augment deterministic MeanFlow with exploration noise. Each transition in the  $K$ -step Markov chain follows:

$$a^{k+1} \sim \mathcal{N}(a^k - \Delta\tau_k \cdot u_\theta(a^k, \tau_{k+1}, \tau_k, o), \sigma^2 I) \quad (6)$$

where  $\tau_k = 1 - k/K$  is the flow time at step  $k$ , and  $\Delta\tau_k = \tau_k - \tau_{k+1} = 1/K$  is the step size.

**Log-Probability.** For PPO, the joint log-probability decomposes over the denoising chain:

$$\log \pi_\theta(a^{0:K} | o) = \log p_0(a^0) + \sum_{k=0}^{K-1} \log \mathcal{N}(a^{k+1} | \mu_k, \sigma^2 I) \quad (7)$$

where  $\mu_k = a^k - \Delta\tau_k \cdot u_\theta(a^k, \tau_{k+1}, \tau_k, o)$ . The full derivation is provided in Appendix C.3 (Eq. 31).

**Training Objective.** We use standard PPO with clipped policy gradient, value loss, and entropy bonus (Schulman et al., 2017), combined with BC regularization to prevent catastrophic forgetting:

$$\mathcal{L}_{\text{BC}} = \mathbb{E}_o \left[ \|a_\omega(o) - a_\theta(o)\|_2^2 \right] \quad (8)$$

where  $a_\omega$  is the action from the frozen pre-trained policy with parameters  $\omega$ . The total fine-tuning objective is:

$$\mathcal{L}_{\text{Stage2}} = \mathcal{L}_{\text{PPO}} + \lambda_{\text{BC}} \mathcal{L}_{\text{BC}} \quad (9)$$

where  $\lambda_{\text{BC}}$  controls the regularization strength (see Eq. 39 for the complete formulation). Detailed algorithms are in Appendix C.3.

## 4. Experiments

We evaluate pre-training and fine-tuning on four RoboMimic manipulation tasks (Mandlekar et al., 2021) and OpenAI Gym locomotion tasks (Brockman et al., 2016), using 100 evaluation episodes per task. To ensure fair comparison with baseline algorithms ReinFlow (Zhang et al., 2025b) and DPPO (Ren et al., 2025), we adopt the same Simplified RoboMimic dataset used in their experiments. Details are provided in Appendix B.

Our experiments are designed to answer three research questions aligned with our contributions:

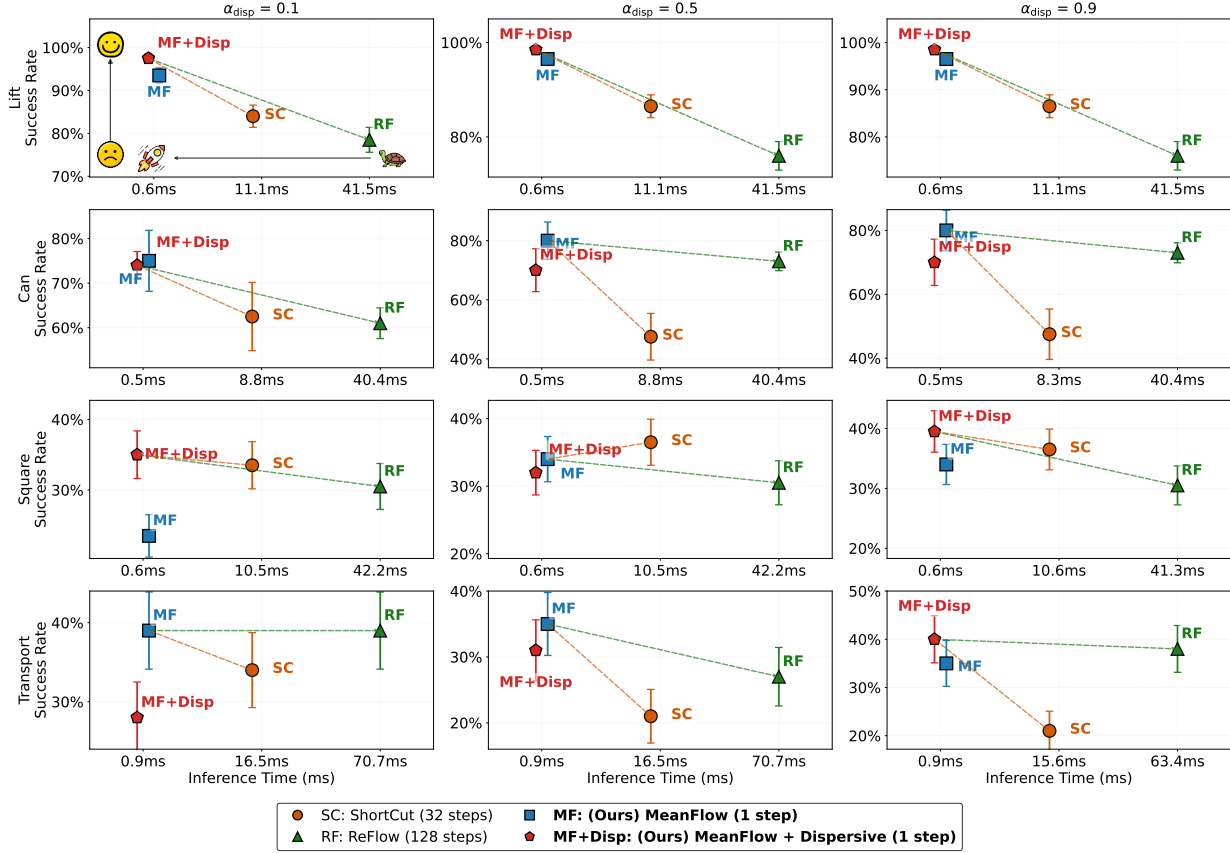


**Figure 3. Stage 1 (Pre-training):** Inference efficiency vs. success rate trade-off across four RoboMimic tasks and three dispersive weights ( $\alpha_{\text{disp}} \in \{0.1, 0.5, 0.9\}$ ). The upper-left region (fast + high success) is ideal. MF and MF+Disp lie on the Pareto frontier, achieving 6–10 $\times$  speedup over ShortCut and 25–40 $\times$  over ReFlow while maintaining superior success rates.

**RQ1:** Can one-step generation match or exceed multi-step diffusion policies while achieving faster inference?

**RQ2:** Is dispersive regularization essential for preventing mode collapse in one-step generation?

**RQ3:** Can online RL fine-tuning push beyond the performance ceiling of offline expert data?

#### 4.1. Stage1: Pre-Training Results of DMPO (RQ1 and RQ2)

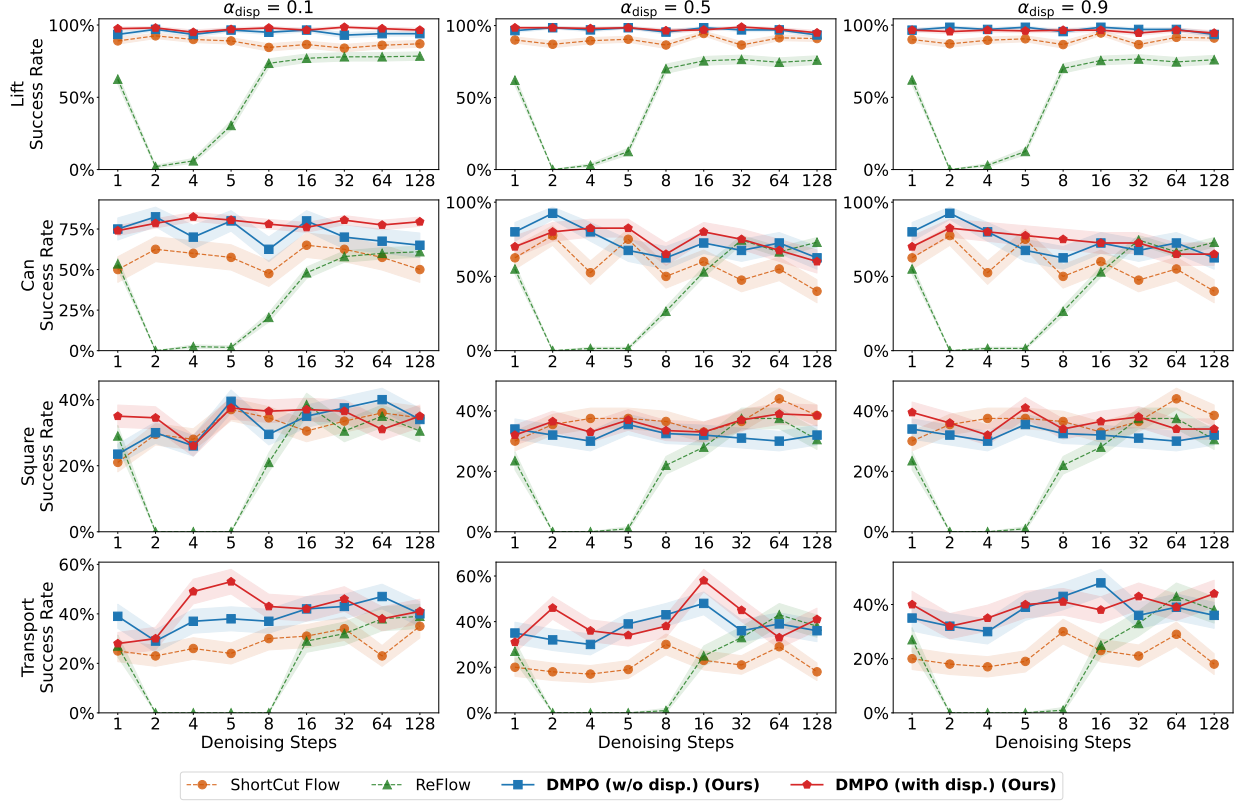
##### 4.1.1. ROBOMIMC PRE-TRAINING TASKS

Figure 3 demonstrates that MeanFlow achieves dramatic inference efficiency gains with **true one-step generation**. Comparing single-sample inference times measured on an NVIDIA RTX 4090 GPU: MF/MF+Disp at 1 step takes only  $\sim 0.6\text{--}1.0\text{ms}$ , while ShortCut at 32 steps takes  $\sim 9\text{--}16\text{ms}$  and ReFlow at 128 steps takes  $\sim 40\text{--}70\text{ms}$ . Our method is **15–20 $\times$  faster** than ShortCut and **60 $\times$  faster** than ReFlow.

More importantly, MF and MF+Disp occupy the **Pareto frontier**, corresponding to the upper-left region in Figure 3:

despite using only a single denoising step, our method achieves competitive or superior success rates compared to baselines that require orders of magnitude more computation. Taking  $\alpha_{\text{disp}} = 0.1$  as an example: on Lift, MF+Disp achieves near-100% success. On Can, both MF and MF+Disp significantly outperform ShortCut and ReFlow. On Transport, MF maintains strong performance while being 60 $\times$  faster than ReFlow.

Figure 4 reveals the effect of dispersive regularization across different denoising steps. ReFlow, shown as green triangles, performs poorly at low steps: on Lift, 1-step success is only  $\sim 60\%$ , requiring 32–64 steps to approach 95%. This indicates that learned vector fields produce highly curved trajectories with large integration errors under few-step sampling. ShortCut, shown as orange circles and designed for few-step inference, improves over ReFlow but exhibits unstable performance with limited ceiling. MF, shown as blue squares, achieves near-saturated performance at 1–5 steps even without dispersive regularization. MF+Disp, shown as red circles, further stabilizes performance, with noticeably reduced variance as evidenced by narrower shaded regions on harder tasks such as Square and Transport.



**Figure 4. Stage 1 (Pre-training):** Success rate vs. denoising steps on a  $4 \times 3$  grid. Rows correspond to Lift, Can, Square, and Transport tasks with increasing difficulty, and columns correspond to  $\alpha_{\text{disp}} \in \{0.1, 0.5, 0.9\}$ . MeanFlow variants, MF and MF+Disp, achieve near-saturated performance at 1–5 steps, while ReFlow and ShortCut require 32–128 steps. Dispersive regularization reduces variance on complex tasks.

The three columns reveal the effect of  $\alpha_{\text{disp}}$ : dispersive regularization consistently improves task success rate across all tested values (0.1, 0.5, 0.9), demonstrating robustness rather than hyperparameter sensitivity. The improvement is more pronounced on complex tasks, confirming that dispersive regularization **prevents representation collapse**, which is essential for stable one-step generation.

We observe a strong linear relationship between success rate improvement and task complexity (Pearson  $r = 0.924$ ), suggesting a simple guideline: increase  $\alpha_{\text{disp}}$  for more challenging tasks. Details are in Appendix A.2.2.

#### 4.1.2. GYM PRE-TRAINING TASKS

Pre-training results on Gym locomotion and Kitchen tasks are reported in the Appendix. Using the same D4RL datasets as ReInFlow, DMPO achieves competitive or superior performance on Hopper, Walker2d, and Kitchen tasks. Notably, DMPO maintains stable performance across inference steps, with clear advantages in the 1–4 step regime: on Hopper, DMPO achieves the best 1-step reward of 1364.1 and 2-step reward of 1484.8. On Kitchen-Complete, DMPO reaches 52.5% at 1-step versus ShortCut’s 35%. These re-

sults confirm that MeanFlow’s few-step sampling advantage generalizes beyond RoboMimic to locomotion and kitchen manipulation domains, while dispersive regularization continues to stabilize performance across different step counts. We additionally report Humanoid pre-training results and note that the Ant performance gap is partly due to dataset version differences between ant-medium-expert-v2 and v0, as discussed in Appendix A.2.1.

#### 4.2. Stage2: Fine-Tuning Results of DMPO (RQ3)

To evaluate the effectiveness of PPO fine-tuning for MeanFlow policies (Contribution 3), we conduct experiments on both RoboMimic manipulation tasks and OpenAI Gym locomotion benchmarks.

##### 4.2.1. ROBOMIMIC FINE-TUNING RESULTS

Figure 5 presents the PPO fine-tuning results on three RoboMimic manipulation tasks: Can, Square, and Transport. We omit Lift as MeanFlow already achieves near-100% success rate during Stage 1 pretraining, leaving no room for improvement via fine-tuning. DMPO achieves competitive or superior performance compared to all baselines while

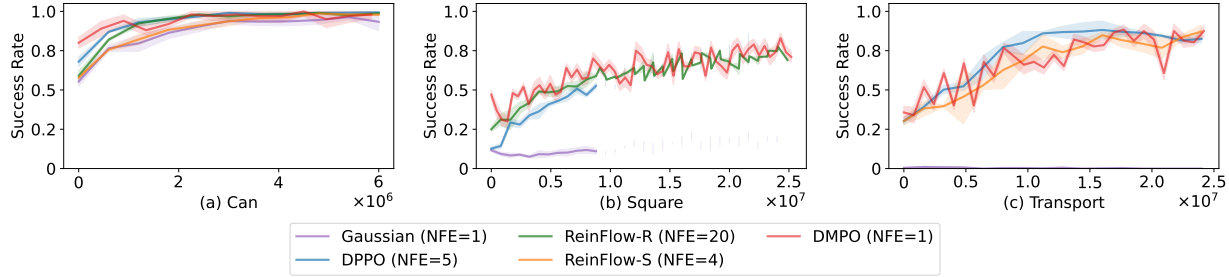


**Figure 5. Stage 2 (PPO Fine-tuning):** Performance on RoboMimic manipulation tasks. MeanFlow in blue is compared with DPPO in yellow, Gaussian in green, ReinFlow-S in red, and ReinFlow-R in purple. Lift is omitted as MeanFlow achieves 100% success during Stage 1 pretraining.

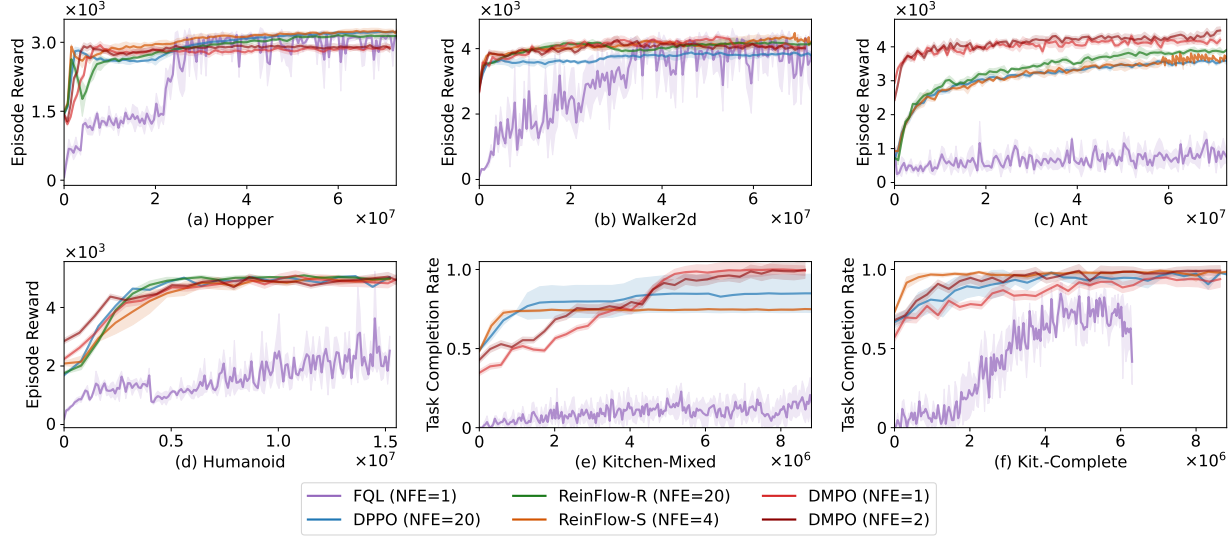


**Figure 6. Stage 2 (PPO Fine-tuning):** Performance on OpenAI Gym locomotion tasks in panels a–d and Kitchen manipulation tasks in panels e–g. MeanFlow in blue is compared with DPPO in yellow, ReinFlow-S in red, ReinFlow-R in purple, and FQL in light blue.

requiring only 1 denoising step. On the **Can** task, DMPO achieves 100% success rate faster than all baselines, outperforming DPPO at 99.3% and ReinFlow-R at 99.0%. On **Square**, DMPO reaches 83% peak success rate, competitive with DPPO at 78.3% and ReinFlow-R at 80%. On **Transport**, DMPO achieves 88% success rate, matching ReinFlow-S performance while significantly outperforming the Gaussian baseline.

#### 4.2.2. OPENAI GYM AND KITCHEN LOCOMOTION RESULTS

We evaluate PPO fine-tuning on four OpenAI Gym locomotion tasks, namely Hopper, Walker2d, Ant, and Humanoid, as well as two Kitchen tasks, Complete and Partial, from D4RL (Fu et al., 2020). As shown in Figure 6, DMPO achieves stable and efficient learning across all tasks while requiring only a single denoising step at inference.

On Gym tasks, DMPO with only 1 denoising step achieves comparable performance to multi-step baselines on Hopper, Walker2d, and Humanoid (Figure 6a, b, d), while signifi-

cantly outperforming all baselines on Ant (Figure 6c).

On Kitchen tasks, which require long-horizon sequential control, DMPO quickly reaches 100% completion on Kitchen-Complete (Figure 6e) and maintains equally strong, stable performance on Kitchen-Mixed and Kitchen-Partial (Figures 6f–g).

Overall, DMPO with one denoising step matches or outperforms multi-step diffusion baselines, including DPPO at 20 steps and ReinFlow at 4 steps, indicating that one-step generation preserves fine-tuning effectiveness. BC regularization with  $\lambda_{BC} = 0.05–0.2$  prevents catastrophic forgetting and enables consistent improvement over the pretrained imitation baseline across diverse task complexities. Detailed comparisons with other one-step generation models and additional baselines are provided in Appendix A.1.

#### 4.3. Physical Robot Experiments

To validate practical applicability, we deploy DMPO on a 7-DOF Franka-Emika-Panda robot equipped with an In-

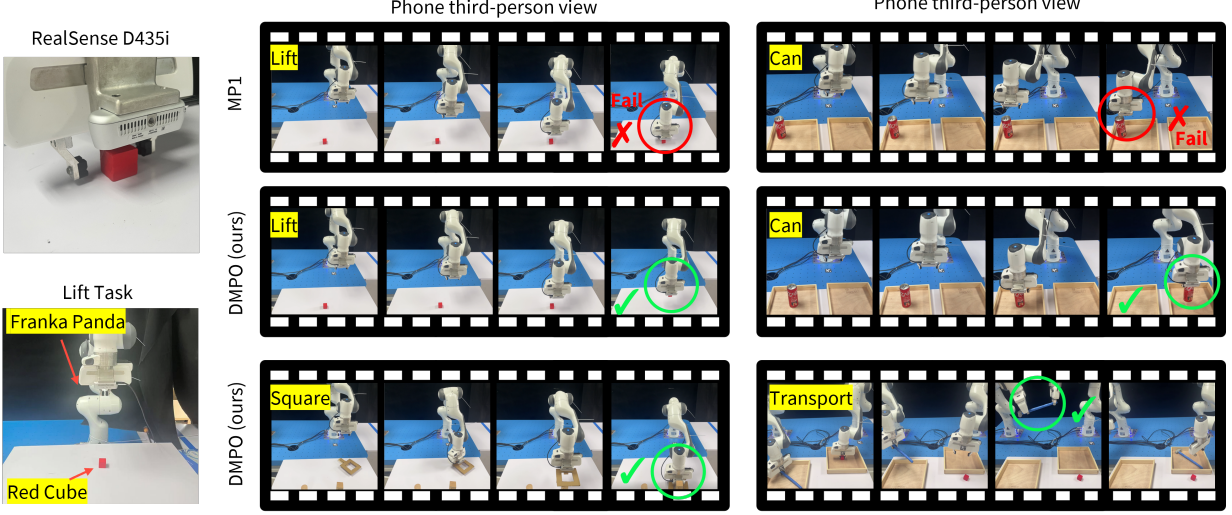


**Figure 7. Real-world deployment of DMPO on a Franka Panda robot.** Left: Hardware setup with Intel RealSense D435i camera for visual observation. Right: Qualitative comparison between MP1 baseline (top row) and our DMPO method (rows 2-3) across four manipulation tasks. MP1 fails on Lift and Can tasks due to imprecise grasping caused by representation collapse, while DMPO successfully completes all four tasks including Square and Transport. These results demonstrate that DMPO’s simulation advantages transfer to physical hardware, validating real-time control capability and sim-to-real generalization. Detailed setup and latency breakdown are in Appendix A.4.

tel RealSense D435i camera across all four RoboMimic tasks. On RTX 2080, DMPO with 1-step inference requires only 2.6ms for neural network forward pass, compared to 12.0ms for 5-step ShortCut and 47.7ms for 20-step ReFlow, achieving 4.6 $\times$  and 18 $\times$  speedup respectively. Including all pipeline stages, DMPO achieves 9.6ms total latency, enabling over 100Hz control frequency.

As shown in Figure 7, we compare MP1 against DMPO on real hardware. We focus on MP1 as it is the only other MeanFlow-based one-step method; other baselines (DPPO, ReinFlow) are compared in simulation, and deploying multi-step methods on real robots incurs significant latency. MP1 fails on Lift and Can tasks due to imprecise grasping caused by representation collapse, while DMPO successfully completes all four tasks including Square and Transport. These results demonstrate that DMPO’s simulation advantages transfer to physical hardware, validating real-time control capability and sim-to-real generalization. Detailed setup and latency breakdown are in Appendix A.4.

#### 4.4. Additional Analysis

We provide additional analysis in Appendix A: comparison with one-step generation baselines demonstrates DMPO achieves superior performance with high data efficiency (Appendix A.1), inference time comparison shows significant speedup over baselines (Appendix A.1.2), and holistic radar comparison confirms top scores across all evaluation dimensions (Appendix A.1.3).

## 5. Conclusion

We presented DMPO, a unified framework that enables real-time robotic control through true one-step generation. By integrating MeanFlow, dispersive regularization, and RL fine-tuning, DMPO achieves both fast inference and high task performance without the efficiency-quality trade-off that limits existing methods. MeanFlow provides mathematically-derived one-step inference without knowledge distillation, while dispersive regularization ensures stable generation by maintaining representation diversity. RL fine-tuning further enables policies to surpass expert demonstrations, breaking through the performance ceiling.

DMPO achieves true real-time robotic control with only **0.6ms inference latency** on RTX 4090. Experiments across RoboMimic manipulation and OpenAI Gym locomotion benchmarks demonstrate near state-of-the-art performance. Compared to vanilla MeanFlow without dispersive regularization, our dispersive regularization improves task success rates by **5–10%**. Furthermore, RL fine-tuning boosts performance by over **50%** compared to behavior cloning pre-training alone. We successfully deployed DMPO on a Franka-Emika-Panda robot, achieving real-time control and validating effective sim-to-real transfer. These results demonstrate that DMPO achieves both fast inference and high task performance, confirming our core claim: **one step is enough** for real-time generative robotic control.

## Impact Statement

This paper presents DMPO, a framework for real-time robotic control through efficient one-step generative policies. By reducing inference latency from hundreds of milliseconds to a few milliseconds, our work enables more responsive and safer human-robot interaction in time-critical applications. The improved efficiency also reduces computational requirements for robot learning, potentially lowering the environmental cost of training robotic systems. We do not anticipate negative societal impacts specific to this work beyond those common to robotics research.

## References

Boffi, N. M., Albergo, M. S., and Vanden-Eijnden, E. Flow map matching. *Transactions on Machine Learning Research (TMLR)*, 2025.

Brockman, G., Cheung, V., Pettersson, L., Schneider, J., Schulman, J., Tang, J., and Zaremba, W. Openai gym. *arXiv preprint arXiv:1606.01540*, 2016.

Chen, H., Zhang, K., Tan, H., Guibas, L., Wetzstein, G., and Bi, S. pi-flow: Policy-based few-step generation via imitation distillation. *arXiv preprint arXiv:2510.14974*, 2025a.

Chen, J. et al.  $\pi_{RL}$ : Online rl fine-tuning for flow-based vision-language-action models. *arXiv preprint arXiv:2510.25889*, 2025b.

Chen, W., Ou, Z., and Li, Y. Neural flow samplers with shortcut models. In *ICLR 2025 Workshop on Foundation Models for Process Intelligence (FPI)*, 2025c.

Chen, X. and He, K. Exploring simple siamese representation learning. In *Proceedings of the IEEE/CVF Conference on Computer Vision and Pattern Recognition (CVPR)*, 2021.

Chi, C., Feng, S., Du, Y., Xu, Z., Cousineau, E., Burchfiel, B., and Song, S. Diffusion policy: Visuomotor policy learning via action diffusion. In *Conference on Robot Learning (CoRL)*, 2023.

Clemente, A. et al. Two-steps diffusion policy for robotic manipulation via genetic denoising. In *Advances in Neural Information Processing Systems (NeurIPS)*, 2025.

Fu, J., Kumar, A., Nachum, O., Tucker, G., and Levine, S. D4rl: Datasets for deep data-driven reinforcement learning. *arXiv preprint arXiv:2004.07219*, 2020.

Geng, Z., Deng, M., Bai, X., Kolter, J. Z., and He, K. Mean flows for one-step generative modeling. In *Advances in Neural Information Processing Systems (NeurIPS)*, 2025a.

Geng, Z. et al. Improved mean flows on the challenges of fast-forward generative models. *arXiv preprint arXiv:2512.02012*, 2025b.

Guo, X. et al. Splitmeanflow: Interval splitting consistency in few-step generative modeling. *arXiv preprint arXiv:2507.16884*, 2025.

Hu, X. et al. Meanflow transformers with representation autoencoders. *arXiv preprint arXiv:2511.13019*, 2025.

Lipman, Y., Chen, R. T. Q., Ben-Hamu, H., Nickel, M., and Le, M. Flow matching for generative modeling. In *International Conference on Learning Representations (ICLR)*, 2023.

Liu, H., Xie, Q., Ye, T., Deng, Z., Chen, C., Tang, S., Fu, X., Lu, H., and Zha, Z.-J. Scott: Accelerating diffusion models with stochastic consistency distillation. In *Proceedings of the AAAI Conference on Artificial Intelligence (AAAI)*, 2025a.

Liu, J., Liu, G., Liang, J., Li, Y., Liu, J., Wang, X., Wan, P., Zhang, D., and Ouyang, W. Flow-grpo: Training flow matching models via online rl. In *Advances in Neural Information Processing Systems (NeurIPS)*, 2025b.

Liu, X., Gong, C., and Liu, Q. Flow straight and fast: Learning to generate and transfer data with rectified flow. In *International Conference on Learning Representations (ICLR)*, 2023.

Lu, G., Gao, Z., Chen, T., Dai, W., Wang, Z., and Tang, Y. Manicm: Real-time 3d diffusion policy via consistency model for robotic manipulation. *arXiv preprint arXiv:2406.01586*, 2024.

Lu, G., Guo, W., Zhang, C., Zhou, Y., Jiang, H., Gao, Z., Tang, Y., and Wang, Z. Vla-rl: Towards masterful and general robotic manipulation with scalable reinforcement learning. *arXiv preprint arXiv:2505.18719*, 2025.

Mandlekar, A., Xu, D., Wong, J., Nasiriany, S., Wang, C., Kulkarni, R., Fei-Fei, L., Savarese, S., Zhu, Y., and Martín-Martín, R. What matters in learning from offline human demonstrations for robot manipulation. In *Conference on Robot Learning (CoRL)*, 2021.

McAllister, D., Ge, S., Yi, B., Kim, C. M., Weber, E., Choi, H., Feng, H., and Kanazawa, A. Flow matching policy gradients. *arXiv preprint arXiv:2507.21053*, 2025.

Nair, A., Dalal, M., Gupta, A., and Levine, S. Awac: Accelerating online reinforcement learning with offline datasets. In *International Conference on Learning Representations (ICLR)*, 2021. *arXiv:2006.09359*.

Peroldi, F., Lynch, C., Wahid, A., Tompson, J., Yu, T., Gu, S. S., Hsu, J., Perona, P., Zeng, A., Dwibedi, D., and Levine, S. Implicit behavioral cloning. In *Conference on Robot Learning (CoRL)*, 2021.

Prasad, A., Lin, K., Wu, J., Zhou, L., and Bohg, J. Consistency policy: Accelerated visuomotor policies via consistency distillation. In *Robotics: Science and Systems (RSS)*, 2024.

Ren, A. Z., Lidard, J., Ankile, L. L., Simeonov, A., Agrawal, P., Majumdar, A., Burchfiel, B., Dai, H., and Simchowitz, M. Diffusion policy policy optimization. In *International Conference on Learning Representations (ICLR)*, 2025.

Schulman, J., Wolski, F., Dhariwal, P., Radford, A., and Klimov, O. Proximal policy optimization algorithms. *arXiv preprint arXiv:1707.06347*, 2017.

Shafiullah, N. M. M., Cui, Z. J., Altanzaya, A., and Pinto, L. Behavior transformers: Cloning  $k$  modes with one stone. In *Advances in Neural Information Processing Systems (NeurIPS)*, 2022.

Sheng, J., Wang, Z., Li, P., and Liu, M. Mp1: Meanflow tames policy learning in 1-step for robotic manipulation. In *Proceedings of the AAAI Conference on Artificial Intelligence (AAAI)*, 2026.

Team, P. I.  $\pi_0$ : A vision-language-action flow model for general robot control. *arXiv preprint arXiv:2410.24164*, 2024.

Team, P. I.  $\pi_{0.5}$ : a vision-language-action model with open-world generalization. In *Proceedings of Machine Learning Research (PMLR)*, 2025.

Wagenmaker, A., Nakamoto, M., Zhang, Y., Park, S., Yagoub, W., Nagabandi, A., Gupta, A., and Levine, S. Steering your diffusion policy with latent space reinforcement learning. In *Conference on Robot Learning (CoRL)*, 2025.

Wang, R. and He, K. Diffuse and disperse: Image generation with representation regularization. *arXiv preprint arXiv:2506.09027*, 2025.

Wang, Z. et al. One-step diffusion policy: Fast visuomotor policies via diffusion distillation. In *International Conference on Machine Learning (ICML)*, 2025.

Yan, X. et al. Maniflow: A general robot manipulation policy via consistency flow training. In *Conference on Robot Learning (CoRL)*, 2025.

Ze, Y., Zhang, G., Zhang, K., Hu, C., Wang, M., and Xu, H. 3d diffusion policy: Generalizable visuomotor policy learning via simple 3d representations. In *Robotics: Science and Systems (RSS)*, 2024.

Zhang, Q., Liu, Z., Fan, H., Liu, G., Zeng, B., and Liu, S. Flowpolicy: Enabling fast and robust 3d flow-based policy via consistency flow matching for robot manipulation. In *Proceedings of the AAAI Conference on Artificial Intelligence (AAAI)*, 2025a.

Zhang, T., Wang, M., Yu, W., Choudhury, S., Garg, A., and Zhao, D. Reinflow: Fine-tuning flow matching policy with online reinforcement learning. In *Advances in Neural Information Processing Systems (NeurIPS)*, 2025b.

Zou, G., Lyu, J., Li, X., and Lu, Z. D2ppo: Diffusion policy optimization with dispersive loss. In *Proceedings of the AAAI Conference on Artificial Intelligence (AAAI)*, 2026.

## Appendix Overview

This appendix provides supplementary material organized as follows:

**Appendix A: Experimental Results** provides comprehensive experimental results including comparative evaluation, Stage 1 pre-training results on RoboMimic and D4RL benchmarks, Stage 2 fine-tuning results, and physical robot experiment details.

**Appendix B: Dataset Analysis and Visualization** presents detailed analysis of dataset selection rationale and distribution characteristics for both RoboMimic and D4RL datasets.

**Appendix C: Algorithm & Method Formulas** contains complete mathematical formulations for Stage 1 MeanFlow pre-training with dispersive regularization and Stage 2 PPO fine-tuning.

**Appendix D: Theoretical Analysis and Unified Framework Design** provides information-theoretic foundation for dispersive regularization and explains the unified framework design that jointly considers model architecture and algorithmic improvements.

## A. Experimental Results

This appendix provides comprehensive experimental results organized by training stage. Section A.1 presents comparative evaluation and validation on RoboMimic, Section A.2 presents Stage 1 pre-training results on Gym and RoboMimic task complexity analysis, Section A.3 presents Stage 2 fine-tuning results on Gym, and Section A.4 details physical robot experiments.

### A.1. Comparative Evaluation and Validation

#### A.1.1. PERFORMANCE COMPARISON ACROSS DATASET VARIANTS

**Dataset Choice.** To ensure fair comparison with baseline algorithms DPPO (Ren et al., 2025) and ReinFlow (Zhang et al., 2025b), we adopt the same Simplified Robomimic MH dataset used in their experiments. For detailed dataset analysis and visualization, see Appendix B.

*Table 1.* Performance Comparison Across Dataset Variants (Multi-Human data). All experiments use the multi-human (mh) dataset variant. Full dataset contains 300 trajectories per task, and Simplified dataset contains 100 trajectories.

Data	Method	Venue	NFE	Dist.	Lift	Can	Square	Transport
<i>Full Dataset (300 trajectories) - Baselines</i>								
Full	LSTM-GMM	CoRL'21 (Mandlekar et al., 2021)	-	✗	0.93	0.81	0.59	0.20
Full	IBC	CoRL'21 (Peroldi et al., 2021)	-	✗	0.02	0.01	0.00	0.00
Full	BET	NeurIPS'22 (Shafullah et al., 2022)	-	✗	0.99	0.90	0.43	0.06
Full	DP-C	RSS'23 (Chi et al., 2023)	100	✗	0.97	0.96	0.82	0.46
Full	DP-T	RSS'23 (Chi et al., 2023)	100	✗	1.00	0.94	0.81	0.35
Full	CP	RSS'24 (Prasad et al., 2024)	3	✓	-	-	0.71	0.37
Full	CP	RSS'24 (Prasad et al., 2024)	1	✓	-	-	0.65	0.38
Full	OneDP-D	ICML'25 (Wang et al., 2025)	1	✓	-	-	0.78	0.71
Full	OneDP-S	ICML'25 (Wang et al., 2025)	1	✓	-	-	0.77	<b>0.72</b>
<i>Simplified Dataset (100 trajectories)</i>								
Simplified	DPPO	ICLR'25 (Ren et al., 2025)	20	✗	1.00	1.00	0.78	0.80
Simplified	ReFlow-R	NeurIPS'25 (Zhang et al., 2025b)	20	✗	1.00	0.99	0.80	-
Simplified	ReFlow-S	NeurIPS'25 (Zhang et al., 2025b)	4	✗	1.00	0.99	-	0.85
Simplified	MP1 <sup>†</sup>	AAAI'26 (Sheng et al., 2026)	1	✗	0.95	0.80	0.35	0.38
Simplified	<b>DMPO (Ours)</b>	-	1	✗	<b>1.00</b>	<b>1.00</b>	<b>0.83</b>	<b>0.88</b>

<sup>†</sup>The original MP1 uses 3D point cloud input, which is not directly applicable to RoboMimic's 2D image observations. Our MP1 results are reproduced using MeanFlow with our lightweight architecture and 2D image input for fair comparison. MP1 is the only other MeanFlow-based one-step method, making it the most direct comparison; deploying multi-step methods on real robots incurs significant latency unsuitable for real-time control. Results for DP-C, DP-T, CP, and OneDP are sourced from (Wang et al., 2025).

**Comparison with One-Step Generation Methods.** Beyond baseline comparisons, we also compare with recent state-of-the-art one-step generation methods, including OneDP (Wang et al., 2025) and Consistency Policy (Prasad et al., 2024). These methods are distilled from multi-step teacher models, so we also include their teacher models (DP-C, DP-T) for reference. As shown in Table 1, DMPO significantly outperforms both existing one-step generation methods and their teacher models. This result is consistent with our theoretical analysis: distilled student models rarely surpass their teachers in performance.

**Data Efficiency.** Notably, Table 1 demonstrates that DMPO using only 1/3 of the official dataset (100 vs. 300 trajectories) can match or even exceed existing one-step generation methods trained on the full dataset. This advantage is particularly pronounced on complex tasks like Transport, where DMPO achieves 88% success rate compared to 72% for OneDP-S, highlighting our algorithm’s superior data utilization efficiency.

**Note on Baselines.** The results for one-step generation baselines (DP-C, DP-T, CP, OneDP) on the full dataset are sourced from (Wang et al., 2025).

**Comparison with MP1.** MP1 (Sheng et al., 2026) is a concurrent work that also explores mean-prediction-based one-step generation. As shown in Table 1, while MP1 achieves reasonable performance on simpler tasks with 95% on Lift and 80% on Can, it struggles significantly on complex manipulation tasks with only 35% on Square and 38% on Transport. In contrast, DMPO substantially outperforms MP1 across all tasks, achieving perfect 100% success rates on Lift and Can, while dramatically improving Square from 35% to 83% and Transport from 38% to 88%. This performance gap highlights the importance of our dispersive regularization in preventing representation collapse, enabling DMPO to maintain high-quality generation even for complex multi-modal action distributions.

#### A.1.2. MODEL ARCHITECTURE AND EFFICIENCY COMPARISON

Table 2 compares model architectures and computational efficiency across different policy learning methods. The first six columns describe model configurations: vision encoder type, action network architecture, parameter count, checkpoint size, and input modality. The last six columns report inference performance on RTX 4090 and RTX 2080 GPUs, including inference time, control frequency, and speedup relative to Diffusion Policy with DDPM sampling at 100 steps.

**Table 2. Model Architecture and Efficiency Comparison.** Comparison of model configurations and inference performance across different policy learning methods: DP (Diffusion Policy (Chi et al., 2023)), CP (Consistency Policy (Prasad et al., 2024)), ReFlow and ShortCut (Zhang et al., 2025b), and MP1 (Sheng et al., 2026). Speedup is computed relative to DP-DDPM (100 steps). All measurements are performed with batch size 1. Note: OneDP (Wang et al., 2025) and 2-DP (Clemente et al., 2025) are not included as their code is not publicly available, preventing accurate inference time measurements.

Model	Vision	Action	Params	Size	Steps	NVIDIA RTX 4090			NVIDIA RTX 2080		
						Time	Freq	Speedup	Time	Freq	Speedup
DP	ResNet-18×2	UNet	281.19M	~4.4GB	100 (DDPM)	391.1ms	2.6Hz	1×	2007.5ms	0.5Hz	1×
					16 (DDIM)	63.7ms	15.7Hz	6×	385.3ms	2.6Hz	5×
					10 (DDIM)	40.3ms	24.8Hz	10×	220.4ms	4.5Hz	9×
CP	ResNet-18×2	UNet	284.86M	~4.4GB	1	5.4ms	187Hz	73×	35.5ms	28Hz	56×
ReFlow	light ViT	MLP	1.78M	~28MB	20	8.4ms	119Hz	46×	47.7ms	21Hz	42×
ShortCut	light ViT	MLP	1.78M	~28MB	5	2.5ms	396Hz	155×	12.0ms	83Hz	167×
MP1	PointNet	UNet	255.80M	~4GB	1	4.1ms	244Hz	96×	21.4ms	47Hz	94×
					2	7.7ms	130Hz	51×	41.6ms	24Hz	48×
					5	18.6ms	54Hz	21×	102.1ms	10Hz	20×
DMPO (Ours)	light ViT	MLP	1.78M	~28MB	1	0.6ms	1770Hz	694×	2.6ms	385Hz	772×
					2	1.1ms	946Hz	371×	4.9ms	204Hz	410×
					5	2.6ms	386Hz	151×	12.0ms	83Hz	167×

Table 2 compares model configurations and inference performance across different methods. The first five columns describe model configurations: vision encoder type, action network architecture, parameter count, and checkpoint size. The last six columns report inference performance on RTX 4090 (for simulation) and RTX 2080 (for physical robot deployment), including inference time, control frequency, and speedup relative to DP-DDPM with 100 steps.

The results reveal that DMPO’s fast inference speed is determined by two factors. First, the lightweight model architecture. UNet-based methods such as DP, CP, and MP1 contain 255–285M parameters, while light ViT+MLP methods such as

ReFlow, ShortCut, and DMPO use only 1.78M parameters. Comparing CP with DMPO under single-step inference on RTX 4090, CP requires 5.4ms while DMPO requires only 0.6ms, demonstrating that the lightweight architecture provides approximately 10 $\times$  speedup. Second, the reduced number of inference steps. Comparing DP-DDIM at 10 steps with DMPO at 1 step, the inference time decreases from 40.3ms to 2.6ms, showing that one-step generation provides approximately 10 $\times$  additional speedup. The combination of these two factors enables DMPO to achieve 694 $\times$  speedup on RTX 4090 and 772 $\times$  speedup on RTX 2080, reaching 1770 Hz and 385 Hz control frequency respectively. The compact 28MB model size also facilitates deployment on resource-constrained robotic platforms.

#### A.1.3. HOLISTIC RADAR COMPARISON

Figure 8 presents a qualitative comparison using radar charts across eight evaluation dimensions: Inference Speed, Model Lightweight, Success Rate, Data Efficiency, Representation Quality, Distillation Free, Beyond Demos, and Training Stability. Each dimension is scored on a 1–5 scale, where 5 indicates excellent performance. We compare DMPO against RL fine-tuning methods including ReinFlow (Zhang et al., 2025b), DPPO (Ren et al., 2025), and  $\pi_{RL}$  (Chen et al., 2025b), as well as generation methods including Diffusion Policy (DP) (Chi et al., 2023), Flow Policy (FP) (Zhang et al., 2025a), 1-DP (Wang et al., 2025), MP1 (Sheng et al., 2026), and Consistency Policy (CP) (Prasad et al., 2024).



**Figure 8. Holistic radar comparison across eight dimensions.** (a) RL fine-tuning methods: DMPO forms the outer envelope, achieving top scores across all dimensions. While ReinFlow and DPPO share the same lightweight architecture and data efficiency as DMPO, they require multi-step inference and show lower representation quality. (b) Generation methods: DMPO outperforms all baselines by combining one-step inference with lightweight architecture, high data efficiency, and the ability to go beyond demonstrations through RL fine-tuning.

**RL Fine-tuning Methods (Panel a).** All RL methods share the ability to surpass demonstrations and remain distillation-free. ReinFlow and DPPO use the same lightweight light ViT+MLP architecture as DMPO with equivalent data efficiency, yet they remain limited by multi-step sampling requirements of 20 and more steps respectively. The  $\pi_{RL}$  method uses a heavier model architecture with lower data efficiency. Only DMPO achieves top scores across all eight dimensions by combining the lightweight architecture with one-step inference capability enabled by our dispersive MeanFlow formulation.

**Generation Methods (Panel b).** The comparison reveals clear trade-offs among existing methods. Multi-step baselines such as DP and FP achieve moderate success rates with stable training, but suffer from slow inference speed and heavy model architectures. Distilled one-step methods including 1-DP and CP accelerate inference but rely on teacher models and cannot surpass demonstration performance. Teacher-free one-step methods like MP1 bypass distillation but suffer from severe representation collapse and use heavy architectures. DMPO stands as the only method achieving top performance across all eight dimensions, demonstrating that our approach successfully resolves the efficiency-stability-adaptability trilemma through the combination of lightweight architecture and advanced algorithm design.

## A.2. Stage 1: Pre-training Results

### A.2.1. STAGE 1: GYM PRE-TRAINING RESULTS

**Table overview.** Table 3 presents pre-training results on OpenAI Gym locomotion tasks including Hopper, Walker2d, Ant, and Humanoid, as well as Franka Kitchen manipulation tasks. For locomotion tasks, we report episode reward, and for Kitchen tasks, we report task completion rate. The table compares DMPO against two baselines from the ReinFlow paper (Zhang et al., 2025b): ReFlow, which uses standard rectified flow, and ShortCut, which uses a reflow-based shortcut model. All baseline results are taken directly from the ReinFlow paper’s open-source data, ensuring fair comparison under identical evaluation protocols. Each row presents a method’s performance across varying inference step counts from 1 to 64 steps, with bold values denoting the best result per step count. The “Impr.” columns show DMPO’s relative improvement over ShortCut, with green indicating improvement and red indicating degradation. We include two DMPO variants for ablation: yellow-highlighted rows indicate DMPO without dispersive regularization, while blue-highlighted rows indicate our full method.

*Table 3. Stage 1 (Pre-training):* Performance comparison of DMPO vs ReinFlow (ReFlow and ShortCut). Locomotion tasks report episode reward, and Kitchen tasks report task completion rate. Best result per task is **bolded**. Green/red Impr. columns show relative improvement over ReFlow at each denoising step.

Task	Method	1	Impr.	2	Impr.	4	Impr.	8	Impr.	16	Impr.	32	Impr.	64	Impr.
<i>Locomotion Tasks (Episode Reward)</i>															
Hopper	ReFlow	1192.6	-	932.4	-	<b>1592.7</b>	-	<b>1584.3</b>	-	1479.1	-	<b>1451.1</b>	-	1389.3	-
	ShortCut	1095.3	-8%	1253.0	+34%	1400.1	-12%	1417.9	-11%	1458.3	-1%	1389.3	-4%	1395.5	0%
	DMPO w/o disp.	1332.7	+12%	1417.6	+52%	<b>1465.2</b>	-8%	1453.0	-8%	1440.9	-3%	1402.9	-3%	1393.5	0%
	DMPO (Ours)	<b>1364.1</b>	+14%	<b>1484.8</b>	+59%	1520.3	-5%	1538.5	-3%	<b>1503.9</b>	+2%	1414.2	-3%	<b>1429.1</b>	+3%
Walker2d	ReFlow	2805.8	-	2810.2	-	2508.4	-	<b>2895.9</b>	-	2944.3	-	2839.7	-	2728.1	-
	ShortCut	<b>2846.5</b>	+1%	2847.4	+1%	<b>2987.3</b>	+19%	2732.5	-6%	2622.2	-11%	2667.8	-6%	2441.4	-11%
	DMPO w/o disp.	2509.8	-11%	2619.0	-7%	2913.9	+16%	2997.6	+4%	2959.7	+1%	2860.3	+1%	<b>3154.6</b>	+16%
	DMPO (Ours)	2606.0	-7%	<b>3033.0</b>	+8%	2777.2	+11%	2831.3	-2%	<b>2953.5</b>	0%	<b>3044.8</b>	+7%	<b>2954.4</b>	+8%
Ant <sup>†</sup>	ReFlow	894.9	-	-40.3	-	495.8	-	654.4	-	709.9	-	761.3	-	771.4	-
	ShortCut	847.4	-5%	779.4	-	685.0	+38%	642.3	-2%	556.2	-22%	544.4	-28%	511.1	-34%
	DMPO w/o disp.	2924.6	+227%	2804.0	-	<b>3355.1</b>	+577%	3302.8	+405%	3427.2	+383%	<b>3434.7</b>	+351%	3371.6	+337%
	DMPO (Ours)	<b>2929.8</b>	+227%	<b>2906.6</b>	-	<b>3289.7</b>	+564%	<b>3377.5</b>	+416%	<b>3352.7</b>	+372%	<b>3267.2</b>	+329%	<b>3536.1</b>	+358%
Humanoid	ReFlow	1655.1	-	1256.7	-	1765.7	-	2106.2	-	2196.2	-	2157.9	-	2156.6	-
	ShortCut	1457.2	-12%	2394.5	+91%	2371.0	+34%	2096.1	0%	2051.0	-7%	1987.9	-8%	2128.5	-1%
	DMPO w/o disp.	2671.6	+61%	3044.0	+142%	<b>3410.4</b>	+93%	<b>3435.5</b>	+63%	3265.9	+49%	2986.2	+38%	2997.0	+39%
	DMPO (Ours)	<b>2588.7</b>	+56%	<b>2809.8</b>	+124%	<b>3070.5</b>	+74%	<b>3235.6</b>	+54%	<b>2928.0</b>	+33%	<b>2823.5</b>	+31%	<b>3097.5</b>	+44%
<i>Kitchen Tasks (Task Completion Rate, %)</i>															
Kitchen-Complete	ReFlow	0%	-	2.5%	-	20.0%	-	50.0%	-	70.0%	-	<b>75.0%</b>	-	77.5%	-
	ShortCut	35.0%	-	42.5%	+1600%	70.0%	+250%	<b>75.0%</b>	+50%	<b>75.0%</b>	+7%	<b>75.0%</b>	0%	77.5%	0%
	DMPO w/o disp.	55.0%	-	<b>72.5%</b>	+2800%	72.5%	+263%	67.5%	+35%	70.0%	0%	67.5%	-10%	65.0%	-16%
	DMPO (Ours)	<b>52.5%</b>	-	<b>70.0%</b>	+2700%	<b>75.0%</b>	+275%	70.0%	+40%	70.0%	0%	70.0%	-7%	70.0%	-10%
Kitchen-Partial	ReFlow	0%	-	5.0%	-	20.0%	-	37.5%	-	35.0%	-	37.5%	-	35.0%	-
	ShortCut	<b>37.5%</b>	-	37.5%	+650%	37.5%	+88%	37.5%	0%	35.0%	0%	35.0%	-7%	37.5%	+7%
	DMPO w/o disp.	35.0%	-	35.0%	+600%	37.5%	+88%	35.0%	-7%	35.0%	0%	32.5%	-13%	35.0%	0%
	DMPO (Ours)	<b>37.5%</b>	-	<b>42.5%</b>	+750%	<b>42.5%</b>	+113%	<b>42.5%</b>	+13%	<b>42.5%</b>	+21%	<b>42.5%</b>	+13%	<b>45.0%</b>	+29%
Kitchen-Mixed	ReFlow	0%	-	2.5%	-	20.0%	-	40.0%	-	42.5%	-	47.5%	-	45.0%	-
	ShortCut	<b>27.5%</b>	-	40.0%	+1500%	42.5%	+113%	40.0%	0%	40.0%	-6%	40.0%	-16%	37.5%	-17%
	DMPO w/o disp.	25.0%	-	37.5%	+1400%	42.5%	+113%	<b>45.0%</b>	+13%	42.5%	0%	42.5%	-11%	42.5%	-6%
	DMPO (Ours)	<b>27.5%</b>	-	<b>42.5%</b>	+1600%	<b>47.5%</b>	+138%	<b>47.5%</b>	+19%	<b>45.0%</b>	+6%	<b>47.5%</b>	0%	<b>47.5%</b>	+6%

<sup>†</sup> Different dataset versions: DMPO uses ant-medium-expert-v2, ReinFlow uses ant-medium-expert-v0.

**Key findings.** The results demonstrate two main conclusions: (1) *DMPO outperforms baseline methods*, particularly in few-step inference scenarios. Across most tasks, DMPO achieves the best or comparable performance at 1-2 steps and maintains superior results at higher step counts. The improvement is especially pronounced on Humanoid and Kitchen-Complete tasks, where DMPO shows substantial gains over both ReFlow and ShortCut. (2) *Dispersive regularization improves performance*.

Comparing DMPO (Ours) against DMPO w/o disp., the full method consistently achieves better results, confirming that dispersive regularization prevents representation collapse and enables more stable generation quality. Note that the Ant task shows a large performance gap due to different dataset versions (see table footnote).

#### A.2.2. STAGE1: TASK COMPLEXITY ANALYSIS OF ROBOMIMIC TESKS

**Table and figure overview.** Table 4 presents task complexity metrics and one-step generation success rates under three dispersive weight configurations ( $\alpha_{\text{disp}} = 0.1, 0.5, 0.9$ ). The “Steps” column shows average trajectory length from expert demonstrations. “Comp.” is the computed complexity score (range 0.1–1.0). “Diff.” indicates qualitative difficulty level. For each  $\alpha_{\text{disp}}$  setting, we compare baseline methods (RF: ReFlow, SC: ShortCut) against our method (MF+Disp), with “Imp.” showing relative improvement over the best baseline. Figure 9 visualizes this data: the left panel plots task complexity against optimal  $\alpha_{\text{disp}}$ , while the right panel shows a heatmap of performance improvements across all task-weight combinations.

**Complexity definition.** We define task complexity using a weighted combination of two factors: (1) trajectory length complexity  $C_{\text{steps}}$ , computed as the min-max normalized logarithm of average steps; and (2) baseline difficulty  $C_{\text{rate}}$ , computed as the min-max normalized inverse of maximum baseline success rate. The final complexity score combines these with equal weighting and rescales to [0.1, 1.0]:  $C_{\text{final}} = 0.1 + 0.9 \times (0.5 \cdot C_{\text{steps}} + 0.5 \cdot C_{\text{rate}})$ .

**Key findings.** Figure 13 shows that trajectory length reflects task complexity: simpler tasks like Lift exhibit concentrated distributions around shorter trajectories, while complex tasks like Transport show wider distributions with significantly longer average lengths. Table 4 further reveals that optimal dispersive weight varies with task complexity. Simpler tasks (Lift, Can) achieve best performance at moderate weights ( $\alpha_{\text{disp}} = 0.5$ ), while more complex tasks (Square, Transport) benefit most from higher weights ( $\alpha_{\text{disp}} = 0.9$ ). Figure 9 quantifies this relationship with a Pearson correlation coefficient of  $r = 0.924$ , confirming that optimal  $\alpha_{\text{disp}}$  increases predictably with task complexity.

Table 4. Stage 1 (Pre-training): Task complexity and performance improvement under different dispersive weights

Task	Steps	Comp.	Diff.	$\alpha_{\text{disp}} = 0.1$				$\alpha_{\text{disp}} = 0.5$				$\alpha_{\text{disp}} = 0.9$			
				Baseline		Ours		Baseline		Ours		Baseline		Ours	
				RF	SC	MF+Disp	Imp.	RF	SC	MF+Disp	Imp.	RF	SC	MF+Disp	Imp.
Lift	108	0.100	Simplest	78.5%	84.0%	97.0%	19.5%	76.0%	86.5%	98.5%	21.7%	76.0%	86.5%	96.0%	18.7%
Can	224	0.428	Medium	61.0%	62.5%	80.5%	30.4%	73.0%	47.5%	82.5%	43.4%	73.0%	47.5%	77.5%	34.7%
Square	272	0.812	High	30.5%	33.5%	37.5%	17.5%	30.5%	36.5%	37.0%	11.3%	30.5%	36.5%	41.0%	23.4%
Trans.	529	0.978	Highest	39.0%	34.0%	53.0%	45.9%	27.0%	21.0%	34.0%	43.9%	38.0%	21.0%	40.0%	47.9%

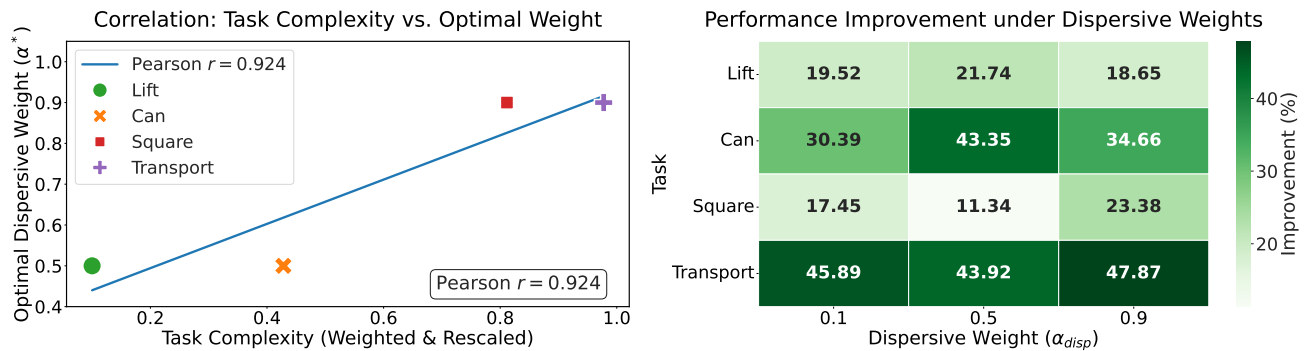


Figure 9. Stage 1 (Pre-training): Performance improvement analysis. Left: Correlation between task complexity and optimal dispersive weight. Right: Heatmap of performance improvement across tasks and weights.

**Practical implications.** The consistent improvement across all  $\alpha_{\text{disp}}$  values in the heatmap demonstrates that dispersive regularization is not hyperparameter-sensitive, and performance improves regardless of the specific value selected. As a practical guideline, we recommend larger  $\alpha_{\text{disp}}$  for more complex tasks. This aligns with our theoretical analysis: complex tasks exhibit more diverse action distributions and thus require stronger representation capacity to avoid mode collapse during one-step generation.

### A.3. Stage 2: Fine-tuning Results

#### A.3.1. WALL-CLOCK TIME OF GYM FINE-TUNING

**Wall-Clock Time Comparison.** To provide a practical perspective on training efficiency, Figure 10 presents wall-clock time comparisons across six Gym tasks. The x-axis uses a non-linear power transformation to emphasize early training dynamics where differences are most pronounced. We compare DMPO with 1-step inference at NFE=1 and 2-step inference at NFE=2 against baseline methods including FQL at NFE=1, DPPO at NFE=20, ReinFlow-R at NFE=4, and ReinFlow-S at NFE=4.

The results demonstrate that DMPO achieves competitive or superior performance while requiring significantly less wall-clock time. On locomotion tasks including Hopper, Walker2d, Ant, and Humanoid, DMPO-1step converges faster than multi-step baselines, benefiting from reduced per-iteration inference cost. Notably, on the Kitchen tasks where success rate is measured, DMPO maintains strong performance with dramatically reduced training time compared to DPPO, which requires 20 denoising steps per action generation.

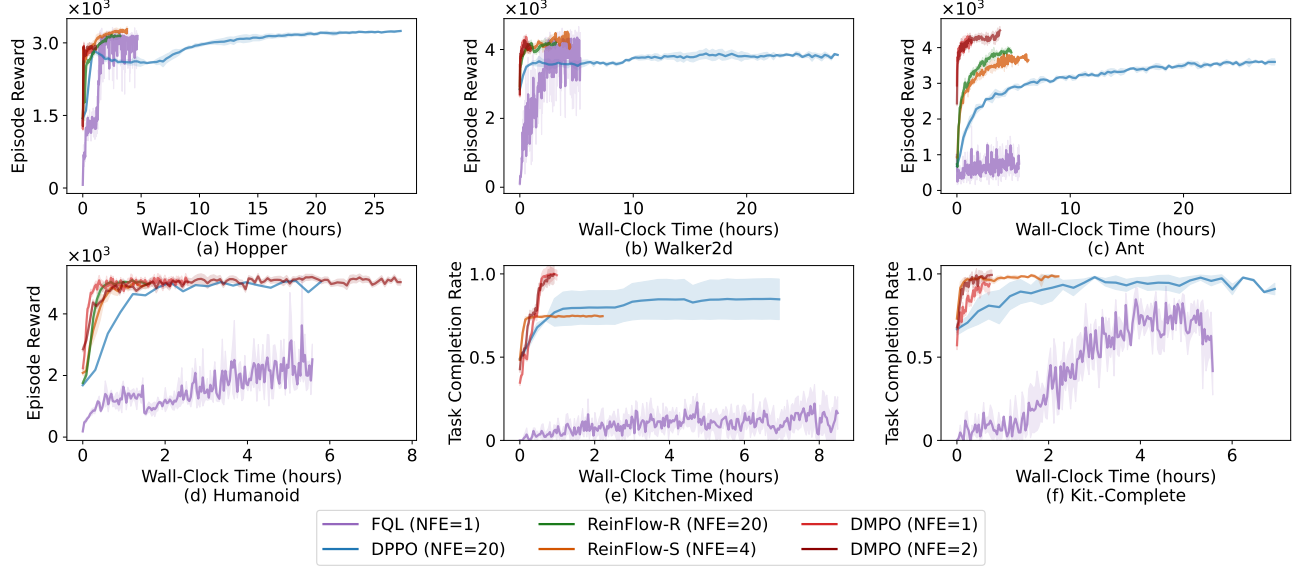


Figure 10. **Stage 2 (PPO Fine-tuning):** Wall-clock time comparison across six Gym tasks. The x-axis shows training time in hours with non-linear scaling to emphasize early training dynamics. DMPO with 1-step and 2-step inference, i.e., NFE=1 and NFE=2, achieves competitive performance while requiring substantially less training time compared to multi-step baselines such as DPPO with NFE=20 and ReinFlow with NFE=4. The efficiency advantage is particularly pronounced on complex tasks like Humanoid and Kitchen environments.

#### A.3.2. BEHAVIOR CLONING LOSS ABLATION

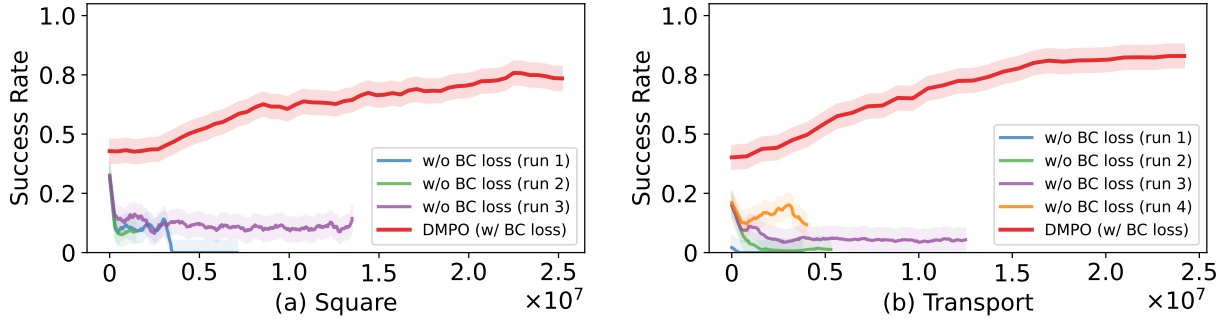


Figure 11. **BC Loss Ablation Study:** Comparison of DMPO with BC loss regularization versus runs without BC loss on RoboMimic Square and Transport tasks. Without BC loss, the policy rapidly collapses, while BC regularization enables stable policy improvement.

We further investigate the role of behavior cloning (BC) loss during RL fine-tuning on RoboMimic tasks. Figure 11 compares

DMPO with BC loss regularization against multiple runs without BC loss on Square and Transport tasks. The results clearly demonstrate that BC loss is critical for stable policy improvement: without BC regularization, the success rate rapidly collapses to near zero across all runs, indicating that the policy deviates too far from the pretrained distribution and loses its learned behavior. In contrast, DMPO with proper BC loss maintains stable learning and achieves high success rates (83% on Square, 87.5% on Transport). This finding aligns with our practical recommendation of applying moderate BC regularization with decay during fine-tuning.

#### A.4. Physical Robot Experiment Details

**Physical Robot Experiment Details** We deploy DMPO on a 7-DOF Franka-Emika-Panda robot equipped with a RealSense D435i wrist-mounted camera at  $96 \times 96 \times 3$  resolution using an NVIDIA RTX 2080 GPU. We compare DMPO against MP1 (MeanFlow Pretrain 1-step without dispersive regularization) to evaluate the effectiveness of our approach. The policy network takes RGB images combined with 9-dimensional robot proprioceptive state including joint positions and gripper state as input, and outputs 7-dimensional actions representing end-effector delta pose, specifically 3D position and 3D orientation, plus gripper command.

Table 5 presents the inference time breakdown for different methods on RTX 2080. Each column represents: Camera (image capture and preprocessing), State (robot state reading), Prep. (input tensor preparation), Inference (neural network forward pass), and Send (action transmission to robot). Notably, the camera preprocessing, which includes color space conversion and normalization operations, is currently executed on the CPU and constitutes the largest latency component (5.4ms). Migrating these operations to GPU can reduce the camera processing time to under 1ms, which would further improve the real-time performance of DMPO to approximately 5ms total latency.

Table 5. Inference time breakdown (ms) for real robot deployment on RTX 2080.

Method	NFE	Camera	State	Prep.	Inference	Send	Total	Freq (Hz)
Reflow	20				47.7		54.7	18.3
Shortcut	5				12.0		19.0	52.6
DMPO	5				12.0		19.0	52.6
DMPO	1				2.6		9.6	104.2

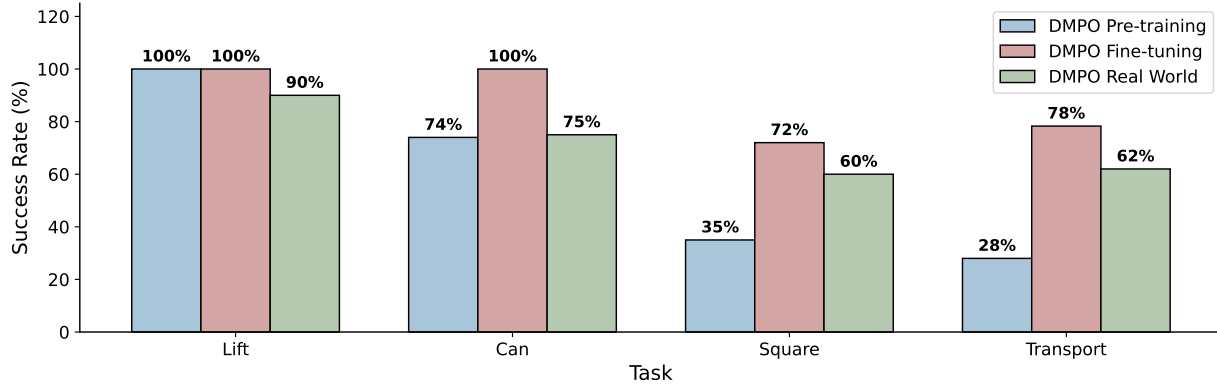


Figure 12. DMPO performance across RoboMimic tasks (NFE=1). We evaluate DMPO at three stages: pre-training, fine-tuning, and real-world deployment. Pre-training establishes baseline performance, fine-tuning significantly improves success rates across all tasks, and real-world experiments demonstrate successful sim-to-real transfer with competitive performance.

Figure 12 summarizes DMPO’s success rates across four RoboMimic tasks at three stages: pre-training, fine-tuning, and real-world deployment. Pre-training with behavior cloning establishes baseline performance, achieving 100% on Lift, 74% on Can, 35% on Square, and 28% on Transport. Fine-tuning with PPO significantly improves performance across all tasks, reaching 100% on both Lift and Can, 72% on Square, and 78% on Transport. Real-world deployment demonstrates successful sim-to-real transfer, with success rates of 90% (Lift), 75% (Can), 60% (Square), and 62% (Transport). These results validate that DMPO’s one-step policy maintains robust performance when deployed on physical hardware.

## B. Dataset Analysis and Visualization

This section provides a comprehensive analysis and visualization of the datasets used in our experiments, addressing potential concerns about dataset choice and ensuring fair comparison with prior work.

### B.1. Dataset Selection and Distribution Analysis

Our codebase is built directly upon DPPO (Ren et al., 2025) and ReinFlow (Zhang et al., 2025b). To ensure fair comparison with these flow-matching baselines, we use the **same simplified RoboMimic pixel dataset** of approximately 1.9 GB released with these works, rather than the full-size RoboMimic image dataset of approximately 78 GB used in the original Diffusion Policy work (Chi et al., 2023). The simplified dataset is the standard benchmark adopted by ReinFlow at NeurIPS 2025 and DPPO at ICLR 2025, ensuring that our performance gains are attributable to the proposed method rather than dataset differences.

**RoboMimic dataset analysis.** Figure 13 compares three dataset variants: Official MH (300 trajectories from multiple humans), Official PH (200 trajectories from proficient humans), and Simple MH (100 trajectories). Panel (a) shows image dataset file sizes, where Transport exhibits the largest data volume with Official MH reaching 31.5GB, while Simple MH remains compact ranging from tens of MB to 1.4GB. Panels (c)–(f) present trajectory length distributions: Lift (c) is the simplest task with average lengths of 48–108 steps, while Transport (f) is the most complex with 469–653 steps. MH datasets exhibit higher variance from multiple demonstrators, PH datasets show lower variance and shorter trajectories, and Simple MH falls between them. This analysis validates our choice of Simple MH as it preserves essential task characteristics while maintaining manageable data volume, demonstrating the task complexity hierarchy: Lift < Can < Square < Transport.

**D4RL dataset analysis.** Figure 14 presents distribution analysis for D4RL gymnasium and Kitchen tasks. Panel (a) shows that Gym locomotion tasks contain approximately 1 million samples each, while Kitchen tasks have fewer samples ranging from 3K to 130K. Panel (b) reveals that Gym tasks have 1000–2000 trajectories compared to only 19–613 for Kitchen tasks. Panel (c) displays episode return distributions, where ant-medium-expert achieves the highest returns with large variance, and Kitchen tasks show lower but more consistent returns. Panel (d) illustrates trajectory length distributions, with Gym tasks around 1000 steps and Kitchen tasks maintaining 200–280 steps. These visualizations demonstrate the diversity of the D4RL benchmark and the multi-modal nature of Kitchen tasks arising from different sub-task sequences.

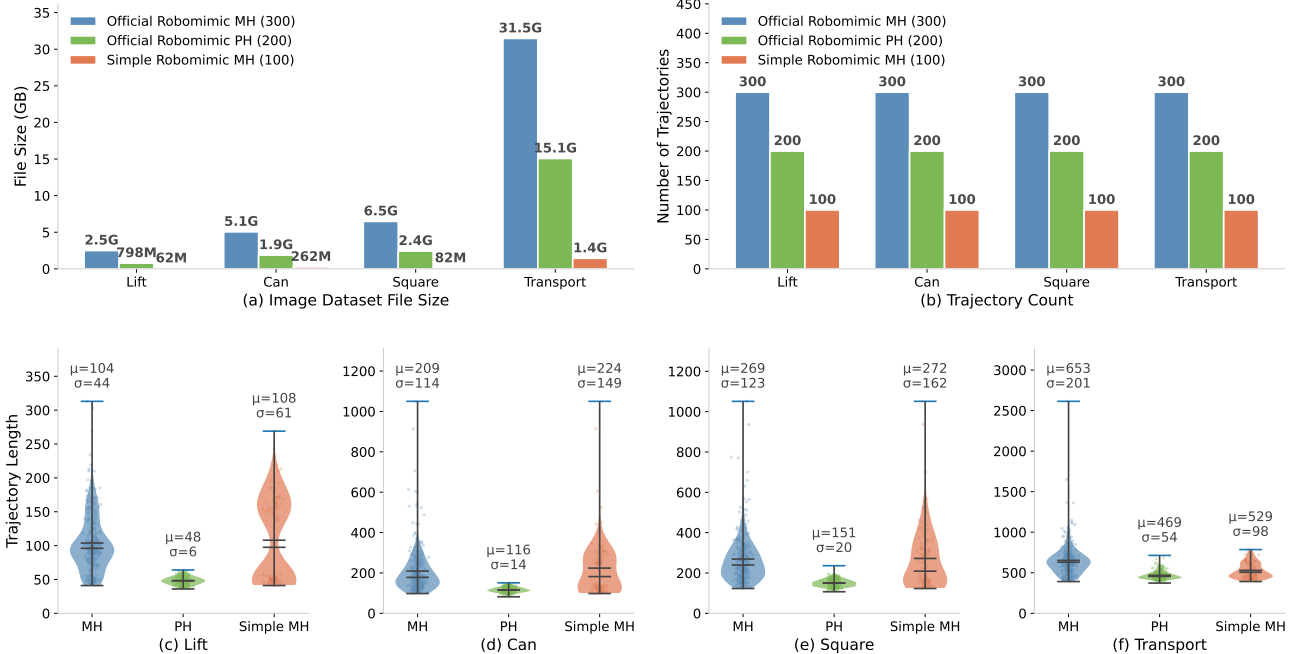


Figure 13. RoboMimic dataset analysis

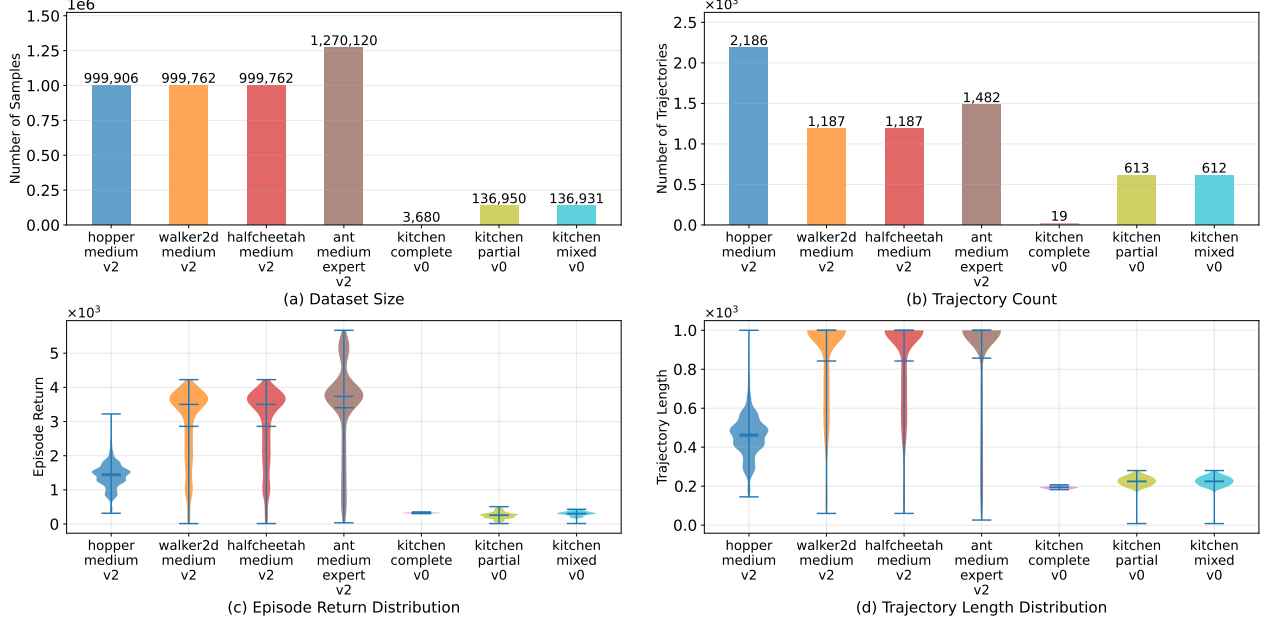


Figure 14. D4RL dataset analysis

## C. Algorithm & Method Formulas

This section presents the core algorithmic components of DMPO: the MeanFlow policy definition, training objectives, inference procedures, and fine-tuning losses.

### C.1. Stage 1: MeanFlow Pre-Training

Stage 1 trains the MeanFlow policy on offline demonstration data using supervised learning. The goal is to learn a velocity network  $u_\theta$  that can transform noise into expert-like actions.

**Notation Adaptation from Original MeanFlow.** To improve readability when combining flow matching with reinforcement learning, we adapt the original MeanFlow notation as shown in Table 6. Our design prioritizes clarity as follows:

**Primary priority:** Distinguishing time-related symbols that are most easily confused, including denoising steps in generative models, continuous flow time, and RL environment time steps. Specifically, we replace the original MeanFlow flow time  $t$  with  $\tau$  to avoid conflict with the standard RL time step  $t$ .

**Secondary priority:** For less critical symbols (flow interval start  $r$  and integration variable  $\xi$ ), we retain  $r$  from the original MeanFlow and use  $\xi$  as the integration dummy variable (since  $\tau$  is now occupied). In Stage 2, RL rewards are distinguished by the time subscript as  $r_t$ .

Table 6. Notation adaptation from original MeanFlow to avoid conflicts with RL symbols.

Concept	Original MeanFlow	This Paper	Reason
Flow time (interval end)	$t$	$\tau$	Avoid conflict with RL time step $t$
Flow time (interval start)	$r$	$r$	Retained (RL reward uses $r_t$ with subscript)
Integration variable	$\tau$	$\xi$	$\tau$ is now used for flow time endpoint
Interpolated state	$z_t$	$z_\tau$	Consistent with $\tau$ notation

**Notation for Pre-Training.** Table 7 summarizes the notation used throughout Stage 1.

**Time convention:**  $\tau = 0$  corresponds to the target action (data), and  $\tau = 1$  corresponds to pure noise. This follows the MeanFlow convention where sampling proceeds from  $\tau = 1$  (noise) to  $\tau = 0$  (action).

Table 7. Stage 1 (Pre-training) notation summary.

Concept	Symbol	Description
Flow time (end)	$\tau \in [0, 1]$	Interval endpoint for flow matching
Flow time (start)	$r \in [0, 1]$	Interval start, $r < \tau$
Observation	$o \in \mathcal{O}$	State from environment/dataset
Action	$a \in \mathbb{R}^{d_a}$	Target action from demonstrations
Noise	$\epsilon \sim \mathcal{N}(0, I)$	Standard Gaussian noise
Interpolated state	$z_\tau$	State at flow time $\tau$ : $z_\tau = (1 - \tau)a + \tau\epsilon$
Velocity network	$u_\theta$	Neural network predicting average velocity
Network parameters	$\theta$	Learnable parameters
Inference steps	$K$	Number of denoising iterations

### Flow Interpolation and Velocity Field.

Flow matching constructs a continuous path from data to noise. Given a target action  $a \in \mathbb{R}^{d_a}$  sampled from the demonstration dataset and Gaussian noise  $\epsilon \sim \mathcal{N}(0, I)$ , we define the **linear interpolation trajectory**:

$$z_\tau = (1 - \tau)a + \tau\epsilon, \quad \tau \in [0, 1] \quad (10)$$

where  $z_\tau \in \mathbb{R}^{d_a}$  represents the intermediate state at flow time  $\tau$ . At  $\tau = 0$ , we have  $z_0 = a$ , corresponding to the target action. At  $\tau = 1$ , we have  $z_1 = \epsilon$ , corresponding to pure noise. The interpolation coefficient  $(1 - \tau)$  controls the action proportion while  $\tau$  controls the noise proportion.

The **instantaneous velocity field**  $v(z_\xi, \xi) : \mathbb{R}^{d_a} \times [0, 1] \rightarrow \mathbb{R}^{d_a}$  describes the rate of change along the flow trajectory at each point. The **average velocity field** over interval  $[r, \tau]$  with  $0 \leq r < \tau \leq 1$  is defined as:

$$u(z_\tau, r, \tau) = \frac{1}{\tau - r} \int_r^\tau v(z_\xi, \xi) d\xi \quad (11)$$

This average velocity represents the mean direction and magnitude of flow over the time interval  $[r, \tau]$ . Importantly, it satisfies the **displacement identity**:

$$(\tau - r) u(z_\tau, r, \tau) = z_\tau - z_r \quad (12)$$

which states that integrating the average velocity over the interval exactly recovers the displacement between  $z_r$  and  $z_\tau$ . This identity is crucial for MeanFlow's ability to perform arbitrary-step inference: by predicting the average velocity  $u$ , we can directly compute the state transition without numerically integrating the instantaneous velocity  $v$ .

**Derivation of the MeanFlow Identity.** We now derive the MeanFlow identity from the displacement identity. Define the cumulative displacement function:

$$F(\tau) = \int_r^\tau v(z_\xi, \xi) d\xi = z_\tau - z_r \quad (13)$$

By the definition of average velocity in Eq. 11, we have:

$$u(z_\tau, r, \tau) = \frac{F(\tau)}{\tau - r} \quad (14)$$

Differentiating with respect to  $\tau$  using the quotient rule:

$$\frac{d}{d\tau} u = \frac{F'(\tau)(\tau - r) - F(\tau) \cdot 1}{(\tau - r)^2} \quad (15)$$

By the fundamental theorem of calculus,  $F'(\tau) = v(z_\tau, \tau)$ . Substituting and simplifying:

$$\begin{aligned} \frac{d}{d\tau} u &= \frac{v(z_\tau, \tau)(\tau - r) - F(\tau)}{(\tau - r)^2} = \frac{v(z_\tau, \tau)}{\tau - r} - \frac{F(\tau)}{(\tau - r)^2} \\ &= \frac{v(z_\tau, \tau)}{\tau - r} - \frac{u}{\tau - r} = \frac{v(z_\tau, \tau) - u}{\tau - r} \end{aligned} \quad (16)$$

Rearranging  $(\tau - r) \frac{d}{d\tau} u = v(z_\tau, \tau) - u$  yields the **MeanFlow identity**:

$$u(z_\tau, r, \tau) = v(z_\tau, \tau) - (\tau - r) \frac{d}{d\tau} u(z_\tau, r, \tau) \quad (17)$$

This identity states that the average velocity equals the instantaneous velocity minus a correction term  $(\tau - r) \frac{d}{d\tau} u$  that accounts for how the average velocity changes over time. When the average velocity is constant, the correction term vanishes and  $u = v$ .

**MeanFlow Training Objective.** The **MeanFlow loss** trains the network to predict the average velocity that transports noise to target actions:

$$\mathcal{L}_{\text{MF}}(\theta) = \mathbb{E}_{(o, a) \sim \mathcal{D}, \epsilon \sim \mathcal{N}(0, I), (r, \tau)} [\|u_\theta(z_\tau, r, \tau, o) - \text{sg}(u_{\text{tgt}})\|^2] \quad (18)$$

where  $\text{sg}(\cdot)$  denotes the **stop-gradient** operator that treats its argument as a constant during backpropagation (Chen & He, 2021),  $\mathcal{D} = \{(o_i, a_i)\}_{i=1}^N$  is the offline demonstration dataset,  $(r, \tau)$  are randomly sampled time interval endpoints with  $0 \leq r < \tau \leq 1$ , and  $z_\tau = (1 - \tau)a + \tau\epsilon$  is the interpolated state (Eq. 10). The network  $u_\theta(z_\tau, r, \tau, o)$  predicts the average velocity over interval  $[r, \tau]$ , and  $u_{\text{tgt}}$  is the **target velocity** derived from the MeanFlow identity.

**Computing the Target Velocity.** Applying the MeanFlow identity (Eq. 17) to training requires computing the total derivative  $\frac{d}{d\tau} u_\theta$ . For linear interpolation, the instantaneous velocity is constant:  $v_\tau = \epsilon - a$ . Since  $u_\theta(z_\tau, r, \tau, o)$  depends on  $\tau$  both explicitly and implicitly through  $z_\tau = (1 - \tau)a + \tau\epsilon$ , we apply the multivariate chain rule:

$$\frac{d}{d\tau} u_\theta(z_\tau, r, \tau, o) = \frac{dz_\tau}{d\tau} \cdot \partial_z u_\theta + \frac{dr}{d\tau} \cdot \partial_r u_\theta + \frac{d\tau}{d\tau} \cdot \partial_\tau u_\theta \quad (19)$$

Substituting  $\frac{dz_\tau}{d\tau} = v_\tau = \epsilon - a$ ,  $\frac{dr}{d\tau} = 0$  (since  $r$  is fixed after sampling), and  $\frac{d\tau}{d\tau} = 1$ :

$$\frac{d}{d\tau} u_\theta(z_\tau, r, \tau, o) = v_\tau \cdot \nabla_z u_\theta + \partial_\tau u_\theta \quad (20)$$

This is the Jacobian-vector product (JVP) between the Jacobian  $[\partial_z u_\theta, \partial_r u_\theta, \partial_\tau u_\theta]$  and the tangent vector  $(v_\tau, 0, 1)$  for inputs  $(z_\tau, r, \tau)$ . Substituting into Eq. 17, the target velocity is:

$$u_{\text{tgt}} = v_\tau - (\tau - r) \frac{d}{d\tau} u_\theta = (\epsilon - a) - (\tau - r) (v_\tau \cdot \nabla_z u_\theta + \partial_\tau u_\theta) \quad (21)$$

Note that  $u_{\text{tgt}}$  depends on the current network  $u_\theta$ , making this a **self-consistent** training objective. The stop-gradient operator  $\text{sg}(\cdot)$  in Eq. 18 is essential: it treats  $u_{\text{tgt}}$  as a fixed target during backpropagation, preventing unstable gradient flow through the JVP term. This is analogous to target networks in DQN or the stop-gradient mechanism in SimSiam (Chen & He, 2021). Once trained, the network enables **one-step generation**: given noise  $z_1 \sim \mathcal{N}(0, I)$ , we directly compute the action as  $a = z_1 - u_\theta(z_1, r=0, \tau=1, o)$ .

For time sampling, we use a **logit-normal distribution** with  $\tau, r = \text{sort}(\text{sigmoid}(\xi_1), \text{sigmoid}(\xi_2))$  where  $\xi_1, \xi_2 \sim \mathcal{N}(0, 1)$ , which concentrates samples in the middle of  $[0, 1]$  and avoids boundary effects. A small fraction ( $\rho = 0.1$ ) of samples set  $r = \tau$  to provide supervision for instantaneous velocity prediction.

## C.2. Stage 1: MeanFlow Pre-Training with Dispersive Regularization

We introduce **dispersive regularization** to prevent **representation collapse**, the phenomenon where the encoder maps distinct observations to nearly identical representations (Wang & He, 2025). Dispersive regularization is particularly important for **one-step generation models**, where the network must directly map noise to diverse actions without iterative refinement. The core idea, analogous to contrastive self-supervised learning, is to encourage internal representations to disperse in the hidden space, but without requiring positive sample pairs.

**Plug-and-play property:** Dispersive regularization is a training-time-only technique. It adds a regularization term to the loss function during pre-training, but **requires no modifications during inference**. Once training is complete, the regularization term is discarded, and the model performs standard MeanFlow sampling. This makes it easy to integrate into existing pipelines without affecting inference speed or architecture.

**Notation.** Let  $B$  denote the batch size and  $\{o_i\}_{i=1}^B$  a batch of observations. We extract intermediate representations from a chosen layer of the velocity network  $u_\theta$ . Following Wang & He (2025), let  $h_i = f_\theta(o_i) \in \mathbb{R}^{d_h}$  denote the flattened intermediate activation for observation  $o_i$ , where  $f_\theta$  represents the subset of layers up to the chosen intermediate block. Each observation produces one representation vector, and we collect them into the batch representation matrix  $\mathbf{H} = [h_1, \dots, h_B]^\top \in \mathbb{R}^{B \times d_h}$ . The temperature hyperparameter  $\tau > 0$  (typically  $\tau = 0.1$ ) controls the sharpness of the dispersive loss.

We provide four variants of dispersive regularization:

**InfoNCE-L2 Loss.** Encourages representations to be far apart in Euclidean distance:

$$\mathcal{L}_{\text{NCE-L2}} = -\frac{1}{B} \sum_{i=1}^B \log \frac{\exp(\|h_i\|_2^2/\tau)}{\sum_{j \neq i} \exp(-\|h_i - h_j\|_2^2/\tau)} \quad (22)$$

The numerator  $\exp(\|h_i\|_2^2/\tau)$  encourages large representation norms, while the denominator penalizes small pairwise distances  $\|h_i - h_j\|_2^2$ . Minimizing this loss pushes representations apart.

**InfoNCE-Cosine Loss.** Encourages representations to have diverse directions (angular separation):

$$\mathcal{L}_{\text{NCE-Cos}} = -\frac{1}{B} \sum_{i=1}^B \log \frac{\exp(1/\tau)}{\sum_{j \neq i} \exp(\text{sim}_{\text{cos}}(h_i, h_j)/\tau)} \quad (23)$$

where the **cosine similarity** between two vectors is:

$$\text{sim}_{\text{cos}}(h_i, h_j) = \frac{h_i^\top h_j}{\|h_i\|_2 \cdot \|h_j\|_2} \in [-1, 1]$$

The constant numerator  $\exp(1/\tau)$  serves as a reference. Minimizing the loss reduces cosine similarities between all pairs, spreading representations uniformly on the hypersphere.

**Hinge Loss.** Directly penalizes pairs that are closer than a margin  $m$ :

$$\mathcal{L}_{\text{Hinge}} = \frac{1}{B(B-1)} \sum_{i=1}^B \sum_{j \neq i} \max(0, m - \|h_i - h_j\|_2) \quad (24)$$

where  $m > 0$  is the margin hyperparameter, typically  $m = 1.0$ , representing the minimum desired distance between any two representations,  $\max(0, \cdot)$  is the hinge function that only penalizes pairs closer than  $m$ , and  $B(B-1)$  is the number of ordered pairs used for normalization.

**Covariance Regularization.** Encourages the covariance matrix of representations to be diagonal with decorrelated features:

$$\mathcal{L}_{\text{Cov}} = \frac{1}{d_h} \sum_{i=1}^{d_h} \sum_{j \neq i} [C(\mathbf{H})]_{ij}^2 \quad (25)$$

where the **sample covariance matrix** is:

$$C(\mathbf{H}) = \frac{1}{B-1} (\mathbf{H} - \bar{\mathbf{H}})^\top (\mathbf{H} - \bar{\mathbf{H}}) \in \mathbb{R}^{d_h \times d_h}$$

with  $\bar{\mathbf{H}} = \frac{1}{B} \sum_{i=1}^B h_i$  being the batch mean broadcast to all rows. The loss penalizes off-diagonal entries  $[C(\mathbf{H})]_{ij}$  for  $i \neq j$ , encouraging feature dimensions to be uncorrelated.

**Combined Stage 1 Objective.** The total Stage 1 training loss combines MeanFlow reconstruction with dispersive regularization:

$$\mathcal{L}_{\text{Stage1}} = \mathcal{L}_{\text{MF}} + \alpha_{\text{disp}} \mathcal{L}_{\text{disp}}(\mathbf{H}^{(\text{Cond})}) \quad (26)$$

where  $\mathcal{L}_{\text{MF}}$  is the MeanFlow velocity prediction loss in Eq. 18,  $\mathcal{L}_{\text{disp}} \in \{\mathcal{L}_{\text{NCE-L2}}, \mathcal{L}_{\text{NCE-Cos}}, \mathcal{L}_{\text{Hinge}}, \mathcal{L}_{\text{Cov}}\}$  is the chosen dispersive regularization applied to the conditional embedding  $\mathbf{H}^{(\text{Cond})}$  output by the Vision Transformer encoder, and  $\alpha_{\text{disp}} > 0$  is the weight balancing reconstruction accuracy vs. representation diversity with typical value  $\alpha_{\text{disp}} = 0.1$ . **DMPO uses InfoNCE-L2 loss by default**, as it achieves the best performance both in the original dispersive regularization study (Wang & He, 2025) and in our experiments on robotic manipulation tasks.

**Inference Procedures.** A key advantage of MeanFlow is that the **same trained network**  $u_{\theta}$  supports arbitrary inference steps  $K \in \{1, 5, 32, 128, \dots\}$  without retraining. This flexibility arises because  $u_{\theta}(z_{\tau}, r, \tau, o)$  is trained to predict the *average velocity over any interval*  $[r, \tau]$ , where  $\tau$  denotes the interval end and  $r$  denotes the interval start, rather than a fixed discretization. At deployment time, we can choose  $K$  based on the available computational budget and required action quality.

Given any step budget  $K \geq 1$ , we partition the unit time interval  $[0, 1]$  into  $K$  equal segments. Define the **time schedule**:

$$1 = \tau_0 > \tau_1 > \tau_2 > \dots > \tau_K = 0, \quad \text{where } \tau_k = 1 - \frac{k}{K}$$

The **multi-step inference** iteratively refines the state from noise to action:

$$z_{\tau_{k+1}} = z_{\tau_k} - (\tau_k - \tau_{k+1}) u_{\theta}(z_{\tau_k}, \tau_{k+1}, \tau_k, o), \quad k = 0, \dots, K-1 \quad (27)$$

where  $z_{\tau_0} = z_1 \sim \mathcal{N}(0, I)$  is the initial sample from standard Gaussian representing pure noise at  $\tau = 1$ ,  $z_{\tau_k} \in \mathbb{R}^{d_a}$  is the intermediate state at step  $k$ ,  $(\tau_k - \tau_{k+1}) = 1/K$  is the time step size,  $u_{\theta}(z_{\tau_k}, \tau_{k+1}, \tau_k, o)$  is the predicted average velocity for interval  $[\tau_{k+1}, \tau_k]$  with the first time argument being the interval start and the second being the interval end, and  $a = z_{\tau_K} = z_0$  is the final action after  $K$  denoising steps.

**Note on time direction:** In flow matching, we construct trajectories from data at  $\tau = 0$  to noise at  $\tau = 1$  during training (i.e.,  $z_{\tau} = (1 - \tau)a + \tau\epsilon$ ). During inference, we reverse this: starting from  $\tau = 1$  corresponding to noise and integrating toward  $\tau = 0$  corresponding to the target action. The update subtracts  $(\tau_k - \tau_{k+1}) \cdot u_{\theta}$  from the current state to move toward the target.

**One-Step Inference ( $K = 1$ ).** The special case  $K = 1$  collapses the entire denoising process into a **single forward pass**:

$$a_{\text{pred}} = z_1 - u_{\theta}(z_1, r=0, \tau=1, o), \quad z_1 \sim \mathcal{N}(0, I) \quad (28)$$

where  $z_1 \sim \mathcal{N}(0, I)$  is the sampled noise serving as the starting point,  $u_{\theta}(z_1, r=0, \tau=1, o)$  is the predicted average velocity over the entire interval  $[0, 1]$  with  $\tau = 1$  as interval end and  $r = 0$  as interval start, and  $a_{\text{pred}} \in \mathbb{R}^{d_a}$  is the predicted action in one step.

This formulation eliminates iterative ODE integration entirely, enabling real-time control at 90Hz or higher. The network directly outputs the full displacement from noise to action, making inference as fast as a standard feedforward network.

**Trade-off:** One-step inference is fastest but may sacrifice some action quality compared to multi-step inference, especially for complex action distributions. The dispersive regularization described in Section C.1 is particularly important for maintaining quality under one-step inference.

### C.3. Stage 2: PPO Fine-Tuning

**Notation for RL Fine-Tuning.** To avoid confusion between environment time steps and flow time, we adopt the following notation convention:  $t$  denotes discrete environment time steps, while  $\tau$  denotes continuous flow time. This distinction is consistent with ReinFlow (Zhang et al., 2025b). **Symbol disambiguation:** The letter  $r$  is used for two distinct concepts: (1) flow interval start  $r$  or  $r_k$  in Stage 1 and the denoising chain, and (2) environment reward  $r_t$ . These are distinguished by context and subscript:  $r$  without subscript or with denoising index  $k$  refers to flow time, while  $r_t$  with environment time subscript  $t$  refers to reward. Table 8 summarizes the notation used in Stage 2.

**Time convention (consistent with Stage 1):** The flow time convention remains the same as in Stage 1:  $\tau = 0$  corresponds to the target action (data), and  $\tau = 1$  corresponds to pure noise. In the discrete setting,  $\tau_0 = 1$  (noise) and  $\tau_K = 0$  (action). Therefore, the denoising chain starts from  $a^0 \sim \mathcal{N}(0, I)$  at  $\tau_0 = 1$  and ends at the final action  $a^K$  at  $\tau_K = 0$ .

**Relation to Stage 1 notation:** In Stage 1 (pre-training), we use continuous flow time  $\tau \in [0, 1]$  and interval start  $r$ , with interpolated state  $z_{\tau} = (1 - \tau)a + \tau\epsilon$ . In Stage 2, the flow time is discretized as  $\tau_k = 1 - k/K$  for denoising step  $k$ , with

Table 8. Stage 2 (RL Fine-tuning) notation summary.

Concept	Symbol	Description
Environment time step	$t$	Step index within an episode
Denoising step	$k$ (superscript)	Step index in the denoising chain
Flow time (end)	$\tau_k = 1 - k/K$	Interval endpoint at step $k$
Flow time (start)	$r_k = \tau_{k+1}$	Interval start at step $k$
Training iteration	$n$	PPO iteration index
Observation	$o_t$	Observation at environment step $t$
Final action	$a_t$	Action executed at step $t$
Intermediate action	$a_t^k$	Action at denoising step $k$
Reward	$r_t$	Reward at environment step $t$
PPO probability ratio	$\rho_t(\theta)$	Ratio of new to old policy

intermediate action  $a^k$  corresponding to  $z_{\tau_k}$ . The interval  $[r, \tau]$  in Stage 1 corresponds to  $[\tau_{k+1}, \tau_k]$  in Stage 2. Within each environment step  $t$ , the denoising chain operates with fixed observation  $o = o_t$ .

Stage 2 fine-tunes the pre-trained MeanFlow policy using online reinforcement learning. We employ Proximal Policy Optimization (PPO), which provides stable policy updates through a clipped surrogate objective. To enable PPO training, we first formulate the multi-step denoising process as a Markov chain with tractable log-probabilities.

**Multi-Step Markov Policy.** MeanFlow formulates action generation as a  $K$ -step Markov chain, enabling tractable probability computation for policy gradient methods. Within a single environment step  $t$ , the observation  $o = o_t$  remains fixed during the entire denoising chain. For notational simplicity, we omit the subscript  $t$  in the following derivations.

**Definition C.1** (Multi-Step Markov Policy). Given an observation  $o$  (i.e.,  $o_t$  at environment step  $t$ ), MeanFlow generates actions via a  $K$ -step denoising process:

$$a^0 \sim p_0(\cdot) = \mathcal{N}(0, I), \quad a^{k+1} \sim \pi_\theta(a^{k+1} | a^k, o), \quad k = 0, \dots, K-1 \quad (29)$$

where  $a^0 \in \mathbb{R}^{d_a}$  is the initial sample from the prior distribution  $p_0 = \mathcal{N}(0, I)$ ,  $a^k \in \mathbb{R}^{d_a}$  denotes the intermediate action at step  $k$  that is progressively refined from noise toward the final action,  $\pi_\theta(a^{k+1} | a^k, o)$  is the learned transition kernel parameterized by  $\theta$ , and  $K \in \mathbb{N}^+$  is the total number of denoising steps such as 1, 5, 32, etc. The final action executed in the environment is  $a := a^K$ .

Each transition in the Markov chain follows a Gaussian distribution centered at the deterministic update:

$$a^{k+1} \sim \mathcal{N}(a^k - \Delta\tau_k \cdot u_\theta(a^k, \tau_{k+1}, \tau_k, o), \sigma^2 I) \quad (30)$$

where  $\tau_k = 1 - k/K$  is the flow time at step  $k$  decreasing from  $\tau_0 = 1$  to  $\tau_K = 0$ ,  $\Delta\tau_k = \tau_k - \tau_{k+1} = 1/K$  is the time step size under uniform partition,  $u_\theta(a^k, \tau_{k+1}, \tau_k, o)$  is the neural network predicting the average velocity over interval  $[\tau_{k+1}, \tau_k]$  conditioned on current state  $a^k$  and observation  $o$  (with the first time argument  $\tau_{k+1}$  being the interval start and the second  $\tau_k$  being the interval end), and  $\sigma^2 > 0$  is the variance of the transition noise, a small hyperparameter typically set to  $\sigma = 0.01$  that ensures the policy has full support for exploration.

The **joint log-probability** of the entire trajectory  $a^{0:K} = (a^0, a^1, \dots, a^K)$  factorizes as:

$$\ln \pi_\theta(a^{0:K} | o) = \ln p_0(a^0) + \sum_{k=0}^{K-1} \ln \mathcal{N}(a^{k+1} | \mu_k, \sigma^2 I) \quad (31)$$

where  $\mu_k = a^k - \Delta\tau_k \cdot u_\theta(a^k, \tau_{k+1}, \tau_k, o)$  is the predicted mean. Each Gaussian log-probability term has the closed form:

$$\ln \mathcal{N}(x | \mu, \sigma^2 I) = -\frac{d_a}{2} \ln(2\pi\sigma^2) - \frac{\|x - \mu\|_2^2}{2\sigma^2}$$

This tractable log-probability enables direct application of policy gradient algorithms like PPO.

**Standard RL notation:** Let  $\gamma \in [0, 1)$  denote the discount factor for future rewards with typical value  $\gamma = 0.99$ , and  $J(\pi_\theta) = \mathbb{E}_{\pi_\theta}[\sum_{t=0}^{\infty} \gamma^t r_t]$  the expected cumulative discounted return. The state value function  $V^\pi(o) = \mathbb{E}_\pi[\sum_{t=0}^{\infty} \gamma^t r_t | o_0 = o]$  estimates expected return from state  $o$ , while the state-action value function  $Q^\pi(o, a) = \mathbb{E}_\pi[\sum_{t=0}^{\infty} \gamma^t r_t | o_0 = o, a_0 = a]$  estimates expected return after taking action  $a$  in state  $o$ . The advantage function  $A^\pi(o, a) = Q^\pi(o, a) - V^\pi(o)$  measures how much better action  $a$  is compared to the average.

**Policy Gradient for Multi-Step Policies.** For MeanFlow's multi-step action generation, we derive a policy gradient that credits the final action's advantage to all intermediate denoising steps.

**Theorem C.2** (Multi-Step Policy Gradient). *Let  $\pi_\theta$  be a MeanFlow policy generating actions via  $K$ -step Markov chain as defined in Eq. 29. The policy gradient is:*

$$\boxed{\nabla_\theta J(\pi_\theta) = \mathbb{E}_{o, a^{0:K} \sim \pi_\theta} \left[ A^{\pi_\theta}(o, a^K) \nabla_\theta \sum_{k=0}^{K-1} \ln \pi_\theta(a^{k+1} | a^k, o) \right]} \quad (32)$$

where  $o$  is an observation sampled during policy rollouts,  $a^{0:K} = (a^0, a^1, \dots, a^K) \sim \pi_\theta(\cdot | o)$  is the full denoising trajectory sampled from the policy,  $A^{\pi_\theta}(o, a^K)$  is the advantage of the **final action**  $a^K$  which is the action actually executed in the environment, and  $\sum_{k=0}^{K-1} \ln \pi_\theta(a^{k+1} | a^k, o)$  is the sum of log-probabilities for all  $K$  transitions.

**Key insight:** The advantage  $A(o, a^K)$  computed from the environment reward for the *final action* is used to update *all* intermediate transition probabilities. This is valid because all transitions contribute to producing the final action: if  $a^K$  yields high reward, we should reinforce the entire denoising chain that produced it.

**PPO Clipped Surrogate Objective.** PPO stabilizes policy updates by limiting the change in action probabilities. Define the **probability ratio**:

$$\rho_t(\theta) = \frac{\pi_\theta(a_t | o_t)}{\pi_{\theta_{\text{old}}}(a_t | o_t)} = \exp(\log \pi_\theta(a_t | o_t) - \log \pi_{\theta_{\text{old}}}(a_t | o_t)) \quad (33)$$

where  $\pi_\theta$  is the current policy being optimized,  $\pi_{\theta_{\text{old}}}$  is the policy used to collect the training data (frozen during optimization), and  $a_t, o_t$  are the action and observation at environment step  $t$  from the collected trajectories.

The **clipped surrogate policy loss** prevents excessively large policy updates:

$$\boxed{\mathcal{L}_{\text{PG}}(\theta) = \mathbb{E}_t [\max(-A_t \cdot \rho_t(\theta), -A_t \cdot \text{clip}(\rho_t(\theta), 1 - \epsilon_{\text{clip}}, 1 + \epsilon_{\text{clip}}))]} \quad (34)$$

where  $A_t$  is the estimated advantage at environment step  $t$  computed using GAE as described below,  $\epsilon_{\text{clip}} > 0$  is the clipping threshold with typical value  $\epsilon_{\text{clip}} = 0.2$ , and  $\text{clip}(x, a, b) = \min(\max(x, a), b)$  clips  $x$  to the interval  $[a, b]$ . The max over the unclipped and clipped objectives ensures that the policy is only updated when it improves the objective, and large deviations from  $\pi_{\theta_{\text{old}}}$  are penalized.

**Generalized Advantage Estimation (GAE):** We estimate advantages using GAE with parameter  $\lambda_{\text{GAE}} \in [0, 1]$ , typically  $\lambda_{\text{GAE}} = 0.95$ :

$$\hat{A}_t = \sum_{\ell=0}^{\infty} (\gamma \lambda_{\text{GAE}})^\ell \delta_{t+\ell}, \quad \text{where } \delta_t = r_t + \gamma V_\theta(o_{t+1}) - V_\theta(o_t)$$

is the TD residual. GAE provides a bias-variance trade-off controlled by  $\lambda_{\text{GAE}}$ . In practice, for a finite episode ending at step  $T$ , this becomes:

$$\hat{A}_t = \sum_{\ell=0}^{T-t-1} (\gamma \lambda_{\text{GAE}})^\ell \delta_{t+\ell}$$

which can be computed efficiently via backward recursion:  $\hat{A}_{T-1} = \delta_{T-1}$  and  $\hat{A}_t = \delta_t + \gamma \lambda_{\text{GAE}} \hat{A}_{t+1}$  for  $t < T-1$ .

**Value Function Loss.** The value network  $V_\theta : \mathcal{O} \rightarrow \mathbb{R}$  estimates expected returns. We train it to minimize the **value loss**:

$$\boxed{\mathcal{L}_V(\theta) = \frac{1}{2} \mathbb{E}_t [(V_\theta(o_t) - R_t)^2]} \quad (35)$$

where  $V_\theta(o_t) \in \mathbb{R}$  is the predicted value for observation  $o_t$ ,  $R_t = \sum_{\ell=0}^{T-t} \gamma^\ell r_{t+\ell}$  is the empirical return representing the discounted sum of rewards from environment step  $t$  to episode end  $T$ , and the factor  $\frac{1}{2}$  simplifies the gradient to  $(V_\theta(o_t) - R_t)$ .

**Entropy Regularization.** To encourage exploration and prevent premature convergence, we add an **entropy bonus**:

$$\mathcal{L}_{\text{ent}}(\theta) = -\mathbb{E}_t[H(\pi_\theta(\cdot | o_t))] \quad (36)$$

where the **entropy** of the policy distribution is:

$$H(\pi_\theta(\cdot | o)) = -\mathbb{E}_{a \sim \pi_\theta(\cdot | o)}[\log \pi_\theta(a | o)]$$

For MeanFlow, since each transition is Gaussian as defined in Eq. 30, the entropy has a closed form:

$$H(\mathcal{N}(\mu, \sigma^2 I)) = \frac{d_a}{2} (1 + \log(2\pi\sigma^2))$$

Minimizing  $\mathcal{L}_{\text{ent}}$ , which has a negative sign, *maximizes* entropy, encouraging diverse action exploration.

**Behavior Cloning Regularization.** To prevent the fine-tuned policy from deviating too far from the pre-trained expert behavior, we add a **behavior cloning** or **BC loss**:

$$\mathcal{L}_{\text{BC}}(\theta) = \mathbb{E}_{o \sim \mathcal{D}_{\text{rollout}}}[\|a_\omega(o) - a_\theta(o)\|_2^2] \quad (37)$$

where  $a_\omega(o) \in \mathbb{R}^{d_a}$  is the action from the **frozen pre-trained policy** with parameters  $\omega$  that remain fixed during fine-tuning,  $a_\theta(o) \in \mathbb{R}^{d_a}$  is the action from the **current fine-tuned policy** with parameters  $\theta$ , and  $\mathcal{D}_{\text{rollout}}$  denotes observations collected during online rollouts. Both policies are evaluated using **identical noise seeds**  $z_1$  to ensure the comparison is meaningful.

The BC coefficient follows a **linear decay schedule** to gradually reduce regularization as learning progresses:

$$\lambda_{\text{BC}}(n) = \begin{cases} \lambda_{\text{BC}}^{\text{init}}, & n < n_{\text{start}} \\ \lambda_{\text{BC}}^{\text{init}} + \frac{n - n_{\text{start}}}{n_{\text{end}} - n_{\text{start}}} (\lambda_{\text{BC}}^{\text{final}} - \lambda_{\text{BC}}^{\text{init}}), & n_{\text{start}} \leq n < n_{\text{end}} \\ \lambda_{\text{BC}}^{\text{final}}, & n \geq n_{\text{end}} \end{cases} \quad (38)$$

where  $n$  is the current training iteration,  $\lambda_{\text{BC}}^{\text{init}}$  is the initial BC weight typically set to 1.0 for strong regularization early,  $\lambda_{\text{BC}}^{\text{final}}$  is the final BC weight typically set to 0.0 to allow full RL optimization, and  $n_{\text{start}}, n_{\text{end}}$  define the iteration range over which the decay occurs.

**Combined Stage 2 Objective.** The total Stage 2 fine-tuning loss combines all components:

$$\mathcal{L}_{\text{Stage2}}(\theta) = \mathcal{L}_{\text{PG}}(\theta) + \lambda_V \cdot \mathcal{L}_V(\theta) + \lambda_{\text{ent}} \cdot \mathcal{L}_{\text{ent}}(\theta) + \lambda_{\text{BC}}(n) \cdot \mathcal{L}_{\text{BC}}(\theta) \quad (39)$$

where  $\mathcal{L}_{\text{PG}}$  is the PPO clipped policy gradient loss in Eq. 34,  $\mathcal{L}_V$  is the value function MSE loss in Eq. 35,  $\mathcal{L}_{\text{ent}}$  is the negative entropy for exploration in Eq. 36, and  $\mathcal{L}_{\text{BC}}$  is the behavior cloning regularization in Eq. 37. The coefficients are  $\lambda_V > 0$  for value loss with typical value  $\lambda_V = 0.5$ ,  $\lambda_{\text{ent}} > 0$  for entropy with typical value  $\lambda_{\text{ent}} = 0.01$ , and  $\lambda_{\text{BC}}(n)$  for the iteration-dependent BC coefficient in Eq. 38. The policy and value networks are updated jointly by minimizing  $\mathcal{L}_{\text{Stage2}}$  using gradient descent, typically with the Adam optimizer.

**Algorithm Pseudocode.**

---

**Algorithm 1** DMPO Stage 1: Pre-Training with Dispersive Regularization

---

**Require:** Dataset  $\mathcal{D} = \{(o, a)\}$ , dispersive weight  $\alpha_{\text{disp}}$

**Ensure:** Trained policy network  $\pi_\theta$

- 1: Initialize network parameters  $\theta$
- 2: **for** each epoch **do**
- 3:   **for** each batch  $\mathcal{B} = \{(o^{(i)}, a^{(i)})\}_{i=1}^B$  **do**
- 4:     Sample  $\epsilon^{(i)} \sim \mathcal{N}(0, I)$  and  $(r^{(i)}, \tau^{(i)})$  from logit-normal
- 5:     Compute interpolants:  $z_\tau^{(i)} = (1 - \tau^{(i)})a^{(i)} + \tau^{(i)}\epsilon^{(i)}$
- 6:     Predict velocity:  $\hat{u}^{(i)} = u_\theta(z_\tau^{(i)}, r^{(i)}, \tau^{(i)}, o^{(i)})$
- 7:     Compute target:  $u_{\text{tgt}}^{(i)} = (\epsilon^{(i)} - a^{(i)}) - (\tau^{(i)} - r^{(i)})\frac{d}{d\tau}u_\theta$  {via JVP, Eq. 21}
- 8:     Extract representations:  $\mathbf{h}^{(i)} = \phi_\theta(o^{(i)})$
- 9:      $\mathcal{L}_{\text{MF}} = \frac{1}{B} \sum_i \|\hat{u}^{(i)} - \text{sg}(u_{\text{tgt}}^{(i)})\|_2^2$  {sg: stop-gradient}
- 10:     $\mathcal{L}_{\text{disp}} = \text{DispersiveLoss}(\{\mathbf{h}^{(i)}\})$
- 11:     $\theta \leftarrow \theta - \eta \nabla_\theta (\mathcal{L}_{\text{MF}} + \alpha_{\text{disp}} \mathcal{L}_{\text{disp}})$
- 12:   **end for**
- 13: **end for**

---



---

**Algorithm 2** DMPO Inference (One-Step or Multi-Step)

---

**Require:** Observation  $o$ , trained policy  $\pi_\theta$ , number of steps  $K$

**Ensure:** Action  $a$

- 1: Sample  $z_1 \sim \mathcal{N}(0, I)$
- 2: **if**  $K = 1$  **then**
- 3:    $a = z_1 - u_\theta(z_1, 0, 1, o)$  {One-step:  $r=0, \tau=1$ }
- 4: **else**
- 5:   **for**  $k = 1$  to  $K$  **do**
- 6:      $\tau_k = 1 - (k - 1)/K, \quad \tau_{k+1} = 1 - k/K$
- 7:      $z_{\tau_{k+1}} = z_{\tau_k} - (\tau_k - \tau_{k+1}) \cdot u_\theta(z_{\tau_k}, \tau_{k+1}, \tau_k, o)$
- 8:   **end for**
- 9:    $a = z_0$
- 10: **end if**

---



---

**Algorithm 3** DMPO Stage 2: PPO Fine-Tuning

---

**Require:** Pre-trained policy  $\pi_\theta$ , environment, hyperparameters  $\lambda_V, \lambda_{\text{ent}}, \lambda_{\text{BC}}$

**Ensure:** Fine-tuned policy  $\pi_\theta$

- 1: **for** iteration  $n = 1, \dots, N_{\text{iter}}$  **do**
- 2:   Collect trajectories  $\{(o_t, a_t^{0:K}, r_t)\}$  using current policy with  $K$ -step sampling
- 3:   Compute GAE advantages  $\{\hat{A}_t\}$  and returns  $\{R_t\}$
- 4:   **for** each PPO epoch **do**
- 5:     Compute probability ratio:  $\rho_t(\theta) = \frac{\pi_\theta(a_t | o_t)}{\pi_{\text{old}}(a_t | o_t)}$
- 6:     Policy loss:  $\mathcal{L}_{\text{PG}} = \mathbb{E}_t[\max(-\hat{A}_t \rho_t, -\hat{A}_t \text{clip}(\rho_t, 1 \pm \epsilon))]$
- 7:     Value loss:  $\mathcal{L}_V = \frac{1}{2} \mathbb{E}_t[(V_\theta(o_t) - R_t)^2]$
- 8:     Entropy loss:  $\mathcal{L}_{\text{ent}} = -\mathbb{E}_t[H(\pi_\theta(\cdot | o_t))]$
- 9:     BC loss:  $\mathcal{L}_{\text{BC}} = \mathbb{E}_t[\|a_\omega(o_t) - a_\theta(o_t)\|_2^2]$
- 10:    Update BC coefficient:  $\lambda_{\text{BC}}(n)$  via linear decay schedule
- 11:    Total loss:  $\mathcal{L} = \mathcal{L}_{\text{PG}} + \lambda_V \mathcal{L}_V + \lambda_{\text{ent}} \mathcal{L}_{\text{ent}} + \lambda_{\text{BC}}(n) \mathcal{L}_{\text{BC}}$
- 12:    Update:  $\theta \leftarrow \theta - \eta \nabla_\theta \mathcal{L}$
- 13:   **end for**
- 14: **end for**

---

## D. Theoretical Analysis and Unified Framework Design

### D.1. Theoretical Analysis of Dispersive Regularization

This subsection provides a rigorous information-theoretic foundation for dispersive regularization, explaining why it effectively prevents representation collapse and improves one-step generation quality.

**Preliminaries and Notation.** Let  $\mathcal{O}$  denote the observation space and  $\mathcal{Z} \subseteq \mathbb{R}^d$  denote the representation space, where  $d$  is the representation dimensionality. The encoder  $f_\theta : \mathcal{O} \rightarrow \mathcal{Z}$  maps observations to  $d$ -dimensional representation vectors. For a batch of  $B$  observations  $\{o_i\}_{i=1}^B$ , we obtain the representation set  $\mathbf{H} = \{\mathbf{h}_i = f_\theta(o_i)\}_{i=1}^B$ . We consider two random variables:

- $O$ : the observation random variable following data distribution  $p(o)$
- $Z = f_\theta(O)$ : the representation random variable with distribution induced by the encoder

We use standard information-theoretic notation:  $I(X; Y)$  denotes the mutual information between random variables  $X$  and  $Y$ ,  $H(X)$  denotes the Shannon entropy of  $X$ , and  $H(X | Y)$  denotes the conditional entropy of  $X$  given  $Y$ .

**The Information Bottleneck Perspective.** From the Information Bottleneck perspective, a good representation  $Z$  should satisfy:

$$\max_{f_\theta} I(Z; A | O) \quad \text{s.t.} \quad I(Z; O) \text{ is maximized} \quad (40)$$

where  $A$  is the target action. The first term requires the representation to contain information necessary for predicting actions, while the second term requires the representation to sufficiently encode observation information. In other words, a good representation  $Z$  should be a sufficient compression of  $O$  while preserving all information needed to predict  $A$ .

**Key Observation:** MeanFlow’s velocity prediction loss  $\mathcal{L}_{\text{MF}}$  only optimizes the first term (prediction accuracy) without explicit constraints on the second term (representation information content). This leaves room for representation collapse, where the model may learn a “shortcut” representation  $Z$  that achieves low prediction loss but discards critical observation information.

**Entropy Decomposition of Mutual Information.** Mutual information can be decomposed as:

$$I(Z; O) = H(Z) - H(Z | O) \quad (41)$$

where  $H(Z) = -\mathbb{E}_{z \sim p(z)}[\log p(z)]$  is the marginal entropy measuring the dispersion of the representation distribution, and  $H(Z | O) = -\mathbb{E}_{o \sim p(o)}[\mathbb{E}_{z \sim p(z|o)}[\log p(z|o)]]$  is the conditional entropy measuring uncertainty in representations given observations.

For a deterministic encoder  $f_\theta$ , given  $o$ , we have  $z = f_\theta(o)$  deterministically, thus  $H(Z | O) = 0$ . This implies:

$$I(Z; O) = H(Z) \quad (42)$$

**Therefore, maximizing mutual information  $I(Z; O)$  is equivalent to maximizing marginal entropy  $H(Z)$ ,** i.e., making the representation distribution as dispersed as possible.

**Why MeanFlow Training Permits Representation Collapse.** The MeanFlow training objective (Eq. 18) can be written as:

$$\mathcal{L}_{\text{MF}}(\theta) = \mathbb{E}_{(o, a), \epsilon, (r, \tau)} [\|u_\theta(z_\tau, r, \tau, o) - u_{\text{tgt}}\|^2] \quad (43)$$

This is a pure regression loss that only constrains velocity prediction accuracy. Consider two extreme cases:

**Case 1: Dispersed Representations.** Different observations  $o_i, o_j$  map to different representations  $\mathbf{h}_i \neq \mathbf{h}_j$ . The velocity network can utilize representation differences to distinguish samples and generate precise conditional velocity predictions.

**Case 2: Collapsed Representations.** All observations map to similar representations  $\mathbf{h}_i \approx \mathbf{h}_j$ , but the velocity network may still achieve low training loss through: (1) overfitting to statistical patterns in training data, (2) exploiting information in time embedding  $\tau$  and noisy state  $z_\tau$ , and (3) compensating for representation information loss in subsequent layers.

Neural network optimization exhibits *implicit regularization*: gradient descent tends to converge to “simple” solutions in parameter space. Collapsed representations correspond to solutions with lower effective complexity because a low-rank covariance matrix means the representation only varies along a few directions while most dimensions remain constant or highly correlated. Without explicit constraints, the optimization process may converge to such degenerate solutions since they require fewer “active” parameters to explain the data.

**Formal Characterization:** Let  $\mu = \mathbb{E}[\mathbf{h}]$  be the mean representation vector and  $\Sigma_{\mathbf{H}} = \mathbb{E}[(\mathbf{h} - \mu)(\mathbf{h} - \mu)^T]$  be the representation covariance matrix. Representation collapse corresponds to  $\text{rank}(\Sigma_{\mathbf{H}}) \ll d$ , meaning most feature dimensions are highly correlated or approximately constant.

**How Dispersive Regularization Maximizes Entropy.** **Entropy Interpretation of InfoNCE-L2 Loss:** The InfoNCE-L2 loss (Eq. 22) is:

$$\mathcal{L}_{\text{NCE-L2}} = -\frac{1}{B} \sum_{i=1}^B \log \frac{\exp(\|\mathbf{h}_i\|_2^2/\tau)}{\sum_{k \neq i} \exp(-\|\mathbf{h}_i - \mathbf{h}_k\|_2^2/\tau)} \quad (44)$$

where  $\tau > 0$  is the temperature parameter controlling the sharpness of the softmax distribution.

Minimizing this loss is equivalent to:

1. **Maximizing the numerator:** Encouraging  $\|\mathbf{h}_i\|_2^2$  to increase, pushing representations away from the origin
2. **Maximizing exponential terms in denominator:** Encouraging  $\|\mathbf{h}_i - \mathbf{h}_k\|_2^2$  to increase, pushing representations of different samples apart

These two effects jointly cause representations to disperse in feature space, corresponding to a high-entropy distribution.

**Connection to Uniform Distribution:** For finite samples, the distribution maximizing discrete entropy  $H(Z)$  is the uniform distribution. For continuous representation spaces, dispersive loss encourages representations to approximately uniformly cover a region of feature space rather than clustering around few points. Let the representation distribution be  $p(z)$  and uniform distribution be  $q(z) = \text{Uniform}(\mathcal{Z})$ . Dispersive loss can be understood as minimizing the distance between  $p(z)$  and some high-entropy reference distribution.

**Entropy Interpretation of Covariance Regularization:** The covariance loss (Eq. 25) is:

$$\mathcal{L}_{\text{Cov}} = \frac{1}{d_h} \sum_{i=1}^{d_h} \sum_{j \neq i} [C(\mathbf{H})]_{ij}^2 \quad (45)$$

where  $d_h$  is the hidden dimension of representations and  $C(\mathbf{H}) \in \mathbb{R}^{d_h \times d_h}$  is the sample covariance matrix computed from the batch  $\mathbf{H}$ . The notation  $[C(\mathbf{H})]_{ij}$  denotes the  $(i, j)$ -th element of this matrix.

This loss penalizes off-diagonal elements of the covariance matrix, encouraging  $C(\mathbf{H})$  to approach a diagonal matrix. For a  $d$ -dimensional Gaussian distribution  $\mathcal{N}(\mu, \Sigma)$  with mean  $\mu$  and covariance  $\Sigma$ , the differential entropy is:

$$H(\mathcal{N}(\mu, \Sigma)) = \frac{1}{2} \log \det(2\pi e \Sigma) = \frac{d}{2} \log(2\pi e) + \frac{1}{2} \sum_{i=1}^d \log \sigma_i^2 \quad (46)$$

where  $\sigma_i^2$  denotes the  $i$ -th eigenvalue of  $\Sigma$  (or the  $i$ -th diagonal element when  $\Sigma$  is diagonal). The second equality follows from the determinant property  $\det(k\mathbf{A}) = k^d \det(\mathbf{A})$  for scalar  $k$  and  $d \times d$  matrix  $\mathbf{A}$ :

$$\det(2\pi e \Sigma) = (2\pi e)^d \det(\Sigma) = (2\pi e)^d \prod_{i=1}^d \sigma_i^2 \quad (47)$$

Taking the logarithm:  $\log \det(2\pi e \Sigma) = d \log(2\pi e) + \sum_{i=1}^d \log \sigma_i^2$ , which yields the formula after multiplying by  $\frac{1}{2}$ .

Geometrically,  $\det(\Sigma)$  represents the volume of the probability concentration region in feature space: larger determinant corresponds to larger volume, meaning the distribution is more spread out and thus has higher entropy. Under fixed

total variance  $\sum_i \sigma_i^2$ , entropy is maximized when the covariance matrix is diagonal, which follows from the AM-GM inequality: the product  $\prod_i \sigma_i^2$  (hence  $\det(\Sigma)$ ) is maximized when all  $\sigma_i^2$  are equal rather than having some large and others small. Decorrelation makes dimensions independent, avoiding information redundancy and thereby maximizing effective information capacity.

**The Combined Training Objective: An Information-Theoretic View.** The DMPO Stage 1 total training objective (Eq. 26) can be understood from an information-theoretic perspective as:

$$\mathcal{L}_{\text{Stage1}} = \underbrace{\mathcal{L}_{\text{MF}}}_{\text{minimize prediction error}} + \alpha_{\text{disp}} \underbrace{\mathcal{L}_{\text{disp}}}_{\text{maximize } H(Z)} \quad (48)$$

According to the Data Processing Inequality, for the Markov chain  $O \rightarrow Z \rightarrow \hat{A}$ , where  $\hat{A}$  denotes the predicted action:

$$I(O; \hat{A}) \leq I(O; Z) = H(Z) \quad (49)$$

The intuition behind this inequality is that information can only decrease (never increase) through processing: when data passes through any transformation, some information may be lost but new information cannot be created. Therefore, maximizing  $H(Z)$  provides an upper bound guarantee on information content for downstream prediction tasks.

**Why One-Step Generation Amplifies the Need for Dispersive Regularization. Error Correction Mechanism in Multi-Step Inference:** Consider  $K$ -step inference where  $K$  is the total number of denoising steps. Let  $\delta_k$  denote the velocity prediction error at step  $k$ , and  $\Delta\tau_k$  denote the time step size at step  $k$ . The cumulative error in the final action is:

$$\epsilon_{\text{total}} = \sum_{k=0}^{K-1} \Delta\tau_k \cdot \delta_k \quad (50)$$

For multi-step inference (large  $K$ ), each step size  $\Delta\tau_k = 1/K$  is small, and subsequent steps can partially correct earlier errors. This provides robustness to degraded representation quality.

**Fragility of One-Step Inference:** For one-step inference ( $K = 1$ ), the entire state transition completes in one step:

$$a = z_1 - u_{\theta}(z_1, r = 0, \tau = 1, o) \quad (51)$$

In this case: (1) step size  $\Delta\tau = 1$  fully amplifies errors, (2) there is no opportunity for iterative correction, and (3) velocity prediction must be accurate in a single pass.

Therefore, one-step inference requires the representation  $\mathbf{h} = f_{\theta}(o)$  to provide sufficiently precise conditional information for the velocity network to generate accurate actions in a single forward pass. When representations collapse, representations of different observations become indistinguishable, and the velocity network cannot generate correct conditional velocity predictions.

**Formal Analysis:** Let  $d_{\text{eff}} = \text{rank}(\Sigma_{\mathbf{H}})$  denote the effective dimensionality of representations, i.e., the number of non-degenerate dimensions in the representation space. For tasks requiring discrimination among  $N$  distinct observation patterns (e.g., different manipulation states or object configurations), theoretically  $d_{\text{eff}} \geq \log_2 N$  is needed to uniquely encode each pattern. Here  $N$  refers to the number of semantically distinct observation categories that the policy must distinguish, not the number of training samples or representation vectors. When  $d_{\text{eff}}$  is sufficient, the representation space has adequate capacity to encode observation differences. However, when collapse causes  $d_{\text{eff}} \ll \log_2 N$ , representations cannot distinguish different observations, and velocity prediction degrades to an average response over all inputs.

**Summary.** MeanFlow's training objective contains only velocity prediction error and lacks constraints on representation structure, making collapsed representations valid local optima. This problem is amplified in few-step inference because limited iteration steps cannot compensate for representation information loss. DMPO addresses this through dispersive regularization, which provides: **(1) Information-Theoretic Guarantee:** Maximizing representation entropy  $H(Z)$  thereby maximizes mutual information  $I(Z; O)$ , ensuring representations sufficiently encode observation information (Eq. 42). **(2) Geometric Effect:** Introducing repulsive potential in feature space prevents representation clustering and maintains distribution uniformity.

## D.2. Unified Framework Design

A potential concern is whether DMPO’s three components (MeanFlow one-step generation, dispersive regularization, and PPO fine-tuning) constitute “technology stacking” without principled integration. This subsection demonstrates that these components form a coherent, interdependent system arising from joint consideration of model architecture and algorithmic design.

**Design Philosophy.** The core goal of DMPO is to achieve real-time robotic control through two architectural considerations: (1) adopting a lightweight model architecture, and (2) reducing the number of sampling steps to one. However, these architectural simplifications alone lead to severe performance degradation on complex tasks. Therefore, we jointly designed algorithmic improvements, including dispersive regularization and PPO fine-tuning, to complement the architectural choices. The theoretical analysis in Appendix C and Section D.1 proves why dispersive regularization is necessary for stable one-step generation, and experimental results validate its effectiveness.

**Functional Dependencies.** The three components exhibit strict functional dependencies where removing any one compromises the entire system. Without dispersive regularization, MeanFlow’s one-step generation suffers from representation collapse, leading to unstable performance on multi-stage tasks. Without one-step generation, multi-step inference increases latency and fails to achieve real-time control; additionally, it drastically reduces PPO training throughput. Without PPO fine-tuning, the policy remains bounded by expert demonstration quality, limiting achievable performance on tasks with suboptimal demonstrations. This interdependence distinguishes DMPO from simple technique combination.

**Validation.** Both theoretical analysis and experimental results confirm the necessity of all components. Ablation studies show that removing any single component significantly reduces task success rate or fails to achieve real-time control inference time. The strong correlation between representation diversity and task success rate validates that dispersive regularization directly enables stable one-step generation. DMPO achieves substantial speedup over multi-step baselines while matching or exceeding their final performance, demonstrating that the joint architecture-algorithm design successfully resolves the efficiency-performance trade-off.